

First fluorescent acetylspermidine deacetylation assay for HDAC10 identifies inhibitors of neuroblastoma cell colony growth that increase lysosome accumulation

*Daniel Herp¹, Johannes Ridinger^{2,3,4}, Dina Robaa⁵, Stephen A. Shinsky^{6,†}, Karin Schmidtkunz¹,
Talha Z. Yesiloglu⁵, Theresa Bayer⁵, Peter Sehr⁷, Nikolas Gunkel^{4,8}, Aubry Miller^{4,8}, David W.
Christianson⁶, Ina Oehme^{2,3,4}, Wolfgang Sippl⁵, Manfred Jung^{*1,9}*

AUTHOR ADDRESS

¹ Institute of Pharmaceutical Sciences, University of Freiburg, Albertstraße 25, 79104 Freiburg, Germany

² Hopp Children's Cancer Center Heidelberg (KiTZ), Im Neuenheimer Feld 280, 69120 Heidelberg, Germany

³ Clinical Cooperation Unit Pediatric Oncology, German Cancer Research Center (DKFZ), Im Neuenheimer Feld 280, 69120 Heidelberg, Germany

⁴ German Cancer Consortium (DKTK), Im Neuenheimer Feld 280, 69120 Heidelberg, Germany

⁵ Institute of Pharmacy, Martin-Luther University of Halle-Wittenberg, 06120 Halle/Saale, Germany

⁶ Roy and Diana Vagelos Laboratories, Department of Chemistry, University of Pennsylvania, 231 South 34th Street, Philadelphia, Pennsylvania 19104-6323, USA

⁷ Chemical Biology Core Facility, European Molecular Biology Laboratory, 69117 Heidelberg, Germany

⁸ Cancer Drug Development Group, Im Neuenheimer Feld 280, 69120 Heidelberg, Germany

⁹ German Cancer Consortium (DKTK), Partner site Freiburg, Hugstetter Str. 55, 79106 Freiburg, Germany

[†]Current address: Department of Biology, The College of New Jersey, 2000 Pennington Road, Ewing, NJ 08618 USA

ABSTRACT

Histone deacetylases (HDACs) are important epigenetic regulators involved in many diseases, esp. cancer. First HDAC inhibitors have been approved for anticancer therapy and many are in clinical trials. Among the 11 zinc-dependent HDACs, HDAC10 has received relatively little attention by drug discovery campaigns, despite its involvement e.g. in the pathogenesis of neuroblastoma. This is due in part to a lack of robust enzymatic conversion assays. In contrast to the protein lysine deacetylase and deacylase activity of the other HDAC subtypes, it has recently been shown that HDAC10 has strong preferences for deacetylation of oligoamine substrates like spermine or spermidine. Hence, it also termed a polyamine deacetylase (PDAC). Here, we present the first fluorescent enzymatic conversion assay for HDAC10 using an aminocoumarin labelled acetyl spermidine derivative to measure its PDAC activity, which is suitable for high-throughput screening. Using this assay, we identified potent inhibitors of HDAC10 mediated spermidine deacetylation in-vitro. Among those are potent inhibitors of neuroblastoma colony growth in culture that show accumulation of lysosomes, implicating disturbance of autophagic flux.

INTRODUCTION

Histone deacetylases are important players in epigenetic regulation.¹⁻⁴ Besides their eponymous deacetylase activity on histones, histone deacetylases (HDACs) have been found to be active on an increasing number of non-histone proteins. One of the most prominent examples is the tumor suppressor protein p53.⁵ Other examples include the cytoskeleton protein α -tubulin and proteins such as SMC3, HSP90 and ERR α .⁶⁻⁹ HDACs are also known as lysine deacetylases (KDACs), a name that better reflects their broad substrate specificity. The 18 known human KDACs are divided into two groups - the classical zinc-dependent enzymes (class I, IIa/b, IV) and the NAD⁺-dependent sirtuins (class III, Sirt1-7). The zinc-dependent enzymes are subdivided into four classes based on phylogenetic analysis: class I consists of HDAC1, 2, 3 and 8; class IIa consists of HDAC4, 5, 7 and 9; class IIb consists of HDAC6 and 10; and class IV consists of only HDAC11.¹⁰ Recently, the substrate specificities of HDAC10 and 11 were redefined: HDAC11 was discovered to be a protein-lysine fatty-acid deacylase¹¹⁻¹² and HDAC10 was discovered to be a polyamine deacetylase (PDAC).¹³ Thus, HDAC10 has important non-protein, non-lysine deacetylase activity.

Regarding their broad range of interaction partners HDACs are involved in many physiological and pathological processes, such as regulation of metabolism,¹⁴⁻¹⁶ aging,¹⁷ gene transcription¹⁸⁻²⁰ and homologous recombination.²¹⁻²² Furthermore, a prominent role in neurodegenerative diseases²³⁻²⁴, metabolic disorders²⁵⁻²⁶ and cancer²⁷⁻²⁹ was reported for this enzyme class. Since only limited treatment options are available for these diseases, HDACs are emerging targets for new therapeutic approaches.

As previously mentioned, the substrate specificity of HDAC10 stands out compared to the other family members. Hai et al. demonstrated that acetylated polyamines are preferred substrates.¹³ The highest catalytic activity was measured for N⁸-acetylspermidine (**1**). Furthermore, acetylputrescine (**2**) and N¹, N⁸-diacetylspermidine (**3**) were deacetylated as well. In contrast, N¹-acetylspermidine (**4**) was converted to a much lesser extent.

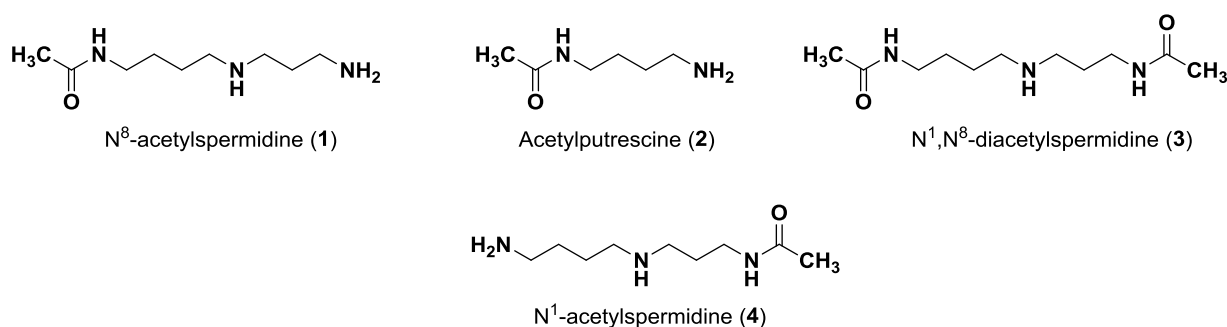


Figure 1: Polyamine substrates of HDAC10

Critical for substrate recognition is a negatively charged glutamate (Glu272 hHDAC10 resp. Glu274 in drHDAC10) at the entrance of the active site, which acts as a gatekeeper to favor the binding of protonated and hence positively charged polyamine substrates. The discrimination of N¹-acetylspermidine against the other polyamine substrates is explained by the position of the positive charge within the molecule. A distance of four to five carbons between the amide moiety and the protonated amine is favorable for the substrate recognition.¹³

In recent years, HDAC10 has been linked to tumor development and proliferation.³⁰⁻³² The development of potential drugs that block HDAC10 has emerged as a new therapeutic strategy, especially for neuroblastoma,^{27, 33-34} but also other disease entities in which HDAC10 is implicated such as lung cancer³⁵⁻³⁶ and ovarian cancer.³⁷ Thus, the therapeutic utility of HDAC10 inhibitors may cover a broad range of indications.

The first HDAC inhibitors (HDACis) Trichostatin A (TSA, **5**) and Trapoxin were reported decades ago.³⁸⁻³⁹ Since Vorinostat (**6**) was approved as the first HDACi for treatment of cutaneous T-cell lymphoma by the FDA three more HDAC inhibitors (Romidepsin (**7**), Belinostat (**8**), Panobinostat (**9**)) got their FDA approval for cancer treatment.⁴⁰⁻⁴⁴ In China one more substance is approved - Tucidinostat (Chidamide, **10**).⁴⁵ Further drug candidates are in clinical trials for cancer treatment. Examples are Quisinostat (**11**), Abexinostat (**12**) and Mocetinostat (**13**).⁴⁶⁻⁴⁸

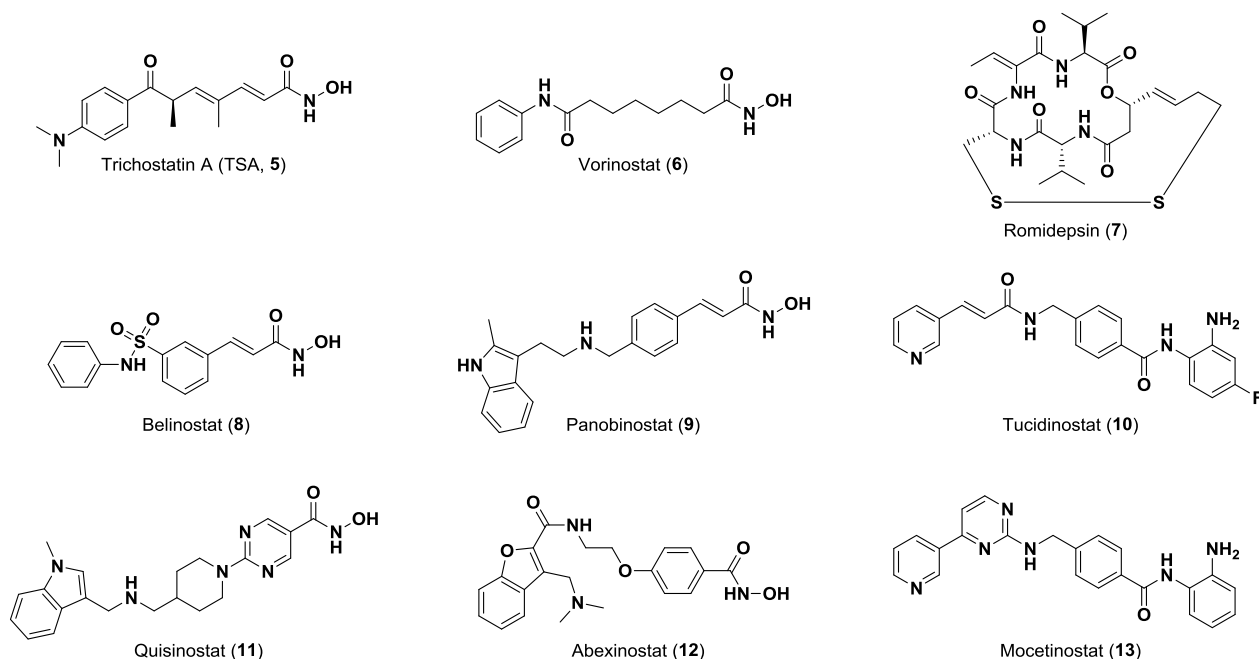


Figure 2: Structures of selected HDAC inhibitors

Many HDAC inhibitors show unselective activity over a wider range of HDAC subtypes. This broad target range has been suggested to be the source of unwanted side effects⁴⁹ and hence an increasing number of subtype selective HDAC inhibitors has been developed as chemical tools and drug candidates.⁵⁰⁻⁵² (reviewed in⁵³)

Suitable assay systems must be available to enable the development of isozyme-selective HDAC inhibitors, but certain isozymes currently lack a facile activity assay. Specifically, due to the newly discovered substrate specificity of HDAC10, the standard HDAC activity assay based on the hydrolysis of an acetyllysine substrate is inappropriate. The fixed-point acetylpolyamine assay developed by Hai and colleagues^{13, 54} employs the polyamine substrate but is not well-suited for high-throughput screening. Only weak lysine deacetylase activity was observed for HDAC10, which increases the risk of false positive results if cell-derived enzyme samples are contaminated with other HDAC isozymes.^{13, 55-56} As an alternative to a substrate conversion assay, two inhibitor based binding assay systems for HDAC10 have been reported in literature. A time resolved fluorescence energy transfer (TR-FRET) *in vitro* assay with recombinant HDAC10 and a bioluminescence energy transfer (BRET) cellular assay were presented.⁵⁷⁻⁵⁸ In both cases the displacement of a fluorescent HDAC10 probe by a competing binder leads to a change of the measured signal. Using these displacement assay systems, G  rally et al. discovered potent HDAC10 hits by testing a set of inhibitors so far being perceived as HDAC6-selective containing Tubastatin A (**14**), HPOB and Nexturastat,⁵⁹ which was not unexpected since both HDAC6 and HDAC10 are class IIb enzymes. Further investigations on Tubastatin A (**14**) and derivatives (**15-17**) identified the basic amine next to the indole structure as crucial for HDAC10 binding, which is consistent with the specificity for polyamine substrates based on the gatekeeper glutamate (see **Figure 3**). Compound **14** and **16** bound strongly to HDAC10 while removing basic properties by substitution of the amine by oxygen (**15**) or by Boc-protection (**17**) led to diminished binding affinity. A salt bridge between the basic amine structure and the gatekeeper residue was postulated for the HDAC10 binders. G  rally et al. assumed an additional flexibility in the L1 loop structure of HDAC10 to be necessary to bind more bulky molecules, such as Tubastatin

A.⁶⁰ While the interaction with the gatekeeper is also reported by Uba et al., the change of the conformation of the L1 loop is not proposed by them.⁶¹⁻⁶²

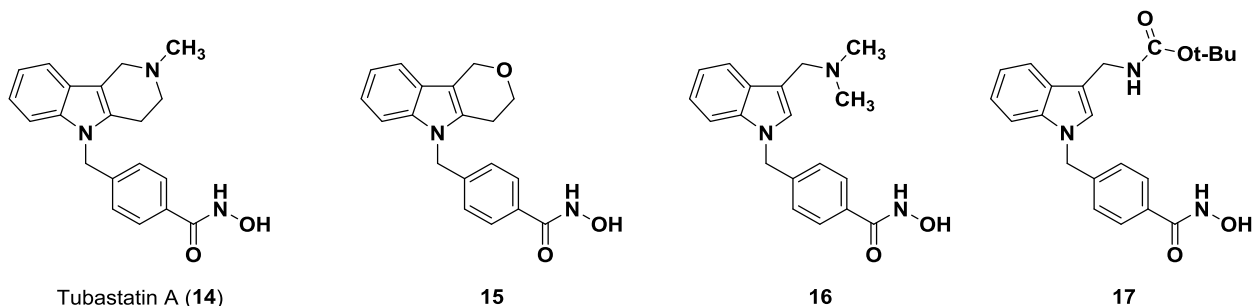


Figure 3: Known HDAC6 (selective) Inhibitor Tubastatin A and analogs. Only compounds with a basic nitrogen near the heterocyclic core (**14**, **16**) exhibit strong HDAC10 binding.

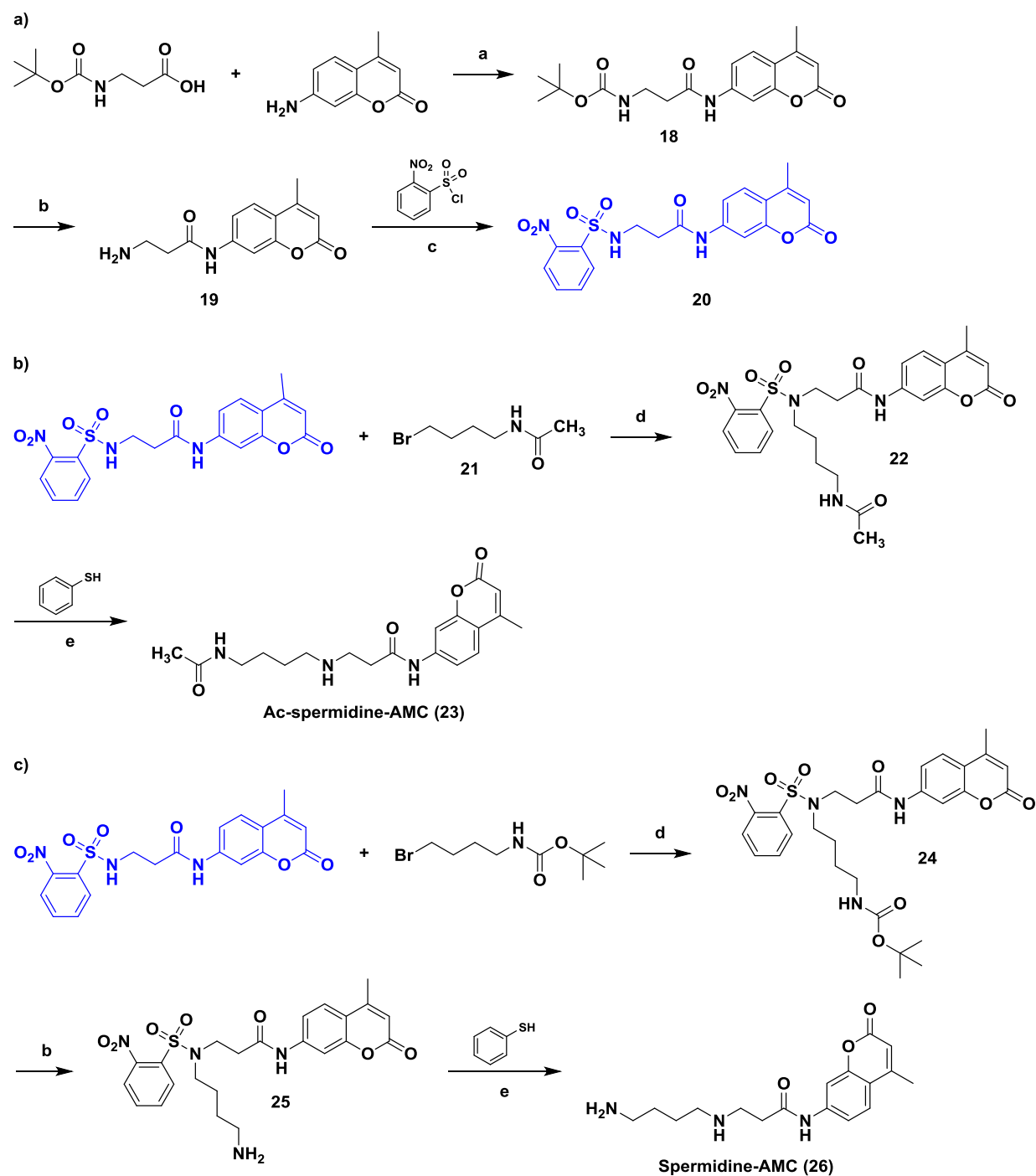
Therefore, we aimed to develop a new HDAC10 activity assay suitable for high-throughput screening. Due to its ease of preparation and its similarity to the human enzyme,^{13, 63} we used HDAC10 from *Danio rerio* (zebrafish) in our assay development studies. Inspired by the discovery that HDAC10 is a polyamine deacetylase,¹³ we developed a new polyamine-based assay substrate suitable for high-throughput activity assays. We used this new assay substrate to screen inhibitor libraries and identified several hits that were subsequently tested in SK-N-BE(2)-C neuroblastoma cells with several compounds resulting in intracellular accumulation of lysosomes and inhibition of colony growth.

RESULTS AND DISCUSSION

SUBSTRATE SYNTHESIS

As outlined above, we set out to synthesize a new HDAC10 substrate based on a polyamine structure and containing a fluorescent moiety. We decided to develop an assay based on an acetylated spermidine derivative. Since N⁸-acetylspermidine and N¹,N⁸-diacetylspermidine were reported to be very well recognized and N¹-acetylspermidine showed a lower affinity to HDAC10, the N⁸-site was chosen to be acetylated while the N¹-site was selected to be modified by a fluorescent reporter group. In **Scheme 1** the synthesis route is depicted. First a building block (**20**) was obtained by an amide coupling of Boc-β-alanine with 7-amino-4-methylcoumarin, followed by Boc deprotection of **18** and nosyl protection of **19** via 2-nitrobenzenesulfonyl chloride. To obtain Ac-spermidine-AMC (**23**), the building block (**20**) was alkylated with N-(4-bromobutyl)acetamide (**21**) to obtain **22**. The nosyl group of **22** was cleaved off by a nucleophilic aromatic substitution with subsequent elimination of SO₂ using thiophenol resulting in the desired substrate **23**. Spermidine-AMC (**26**), the deacetylated substrate, was synthesized in three steps from the building block **20**; an alkylation of **20** with 4-(Boc-amino)butylbromide to **24**, followed by Boc deprotection to **25**, the nosyl deprotection of **25** leads finally to the Spermidine-AMC (**26**).

Scheme 1. Synthesis of a protected amino propionyl aminocumarin (**a**), Ac-spermidine-AMC (**23**) (**b**) and Spermidine-AMC (**26**) (**c**)



SUBSTRATE VALIDATION

With the substrate in hand we aimed to develop an homogeneous assay. To initially confirm the chemistry behind the desired final one-pot format (see below), we monitored conversion of the assay substrate Ac-spermidine-AMC (**23**) by HDAC10 using HPLC. Direct detection of the metabolite **26** via HPLC was not possible. Therefore, an derivatization of **26** with fluorescamine as an amine derivatization agent (which only reacts with the deacetylated product) was done and the metabolite-fluorescamine adduct was measured. Retention times of the **23** (11.5 min, method see experimental), the fluorescamine adduct (16.8 min) and fluorescamine (22.3 min) were determined (see **Figure S1**). A dilution series of the substrate (**23**) and the expected metabolite (**26**) were balanced to a concentration of 100 μM and fluorescamine was added and a calibration curve was generated (**Figure 4a**, **Table S1**). The linear calibration curve demonstrated the potential to measure deacetylation in the desired concentration range.

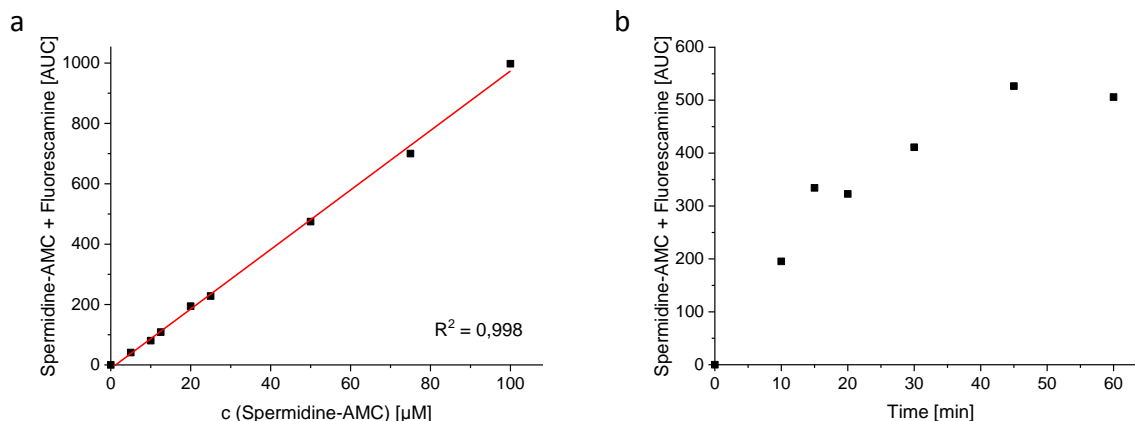


Figure 4: Proof of substrate conversion by HPLC: a) Calibration curve of Spermidine-AMC, detection via derivatization with fluorescamine; b) Conversion of Ac-spermidine-AMC by drHDAC10: incubation for 0-60 min in buffer (20 mM Na_2HPO_4 , pH 7.9, 10 mM NaCl, 0.25 mM EDTA). Reaction was stopped by adding fluorescamine in acetonitrile. Detection of conversion by HPLC with UV-detector at 210 nm.

To monitor enzymatic substrate conversion, Ac-spermidine-AMC was incubated with drHDAC10 (0.027 mg/mL) in buffer (20 mM Na₂HPO₄, pH 7.9, 10 mM NaCl, 0.25 mM EDTA). The reaction was stopped at different time points (0, 10, 15, 20, 30, 45, 60 min) by adding fluorescamine in acetonitrile. From time point “10 min” a new peak with a retention time of 16.8 min, the expected derivatized metabolite, appeared. An increase of the metabolite until time point 45 min was observed and conversion was maximal around a level of about 50 % (**Figure 4b**). Using the fluorescamine detection and HPLC, we could thus show that **23** is a competent substrate of drHDAC10, and that it is converted to **26**.

HOMOGENEOUS ASSAY FORMAT

In a next step, we monitored the enzymatic conversion in a microplate-based assay design. Measurement in a plate reader format enables high-throughput screening. We wanted to use naphthalene-2,3-dialdehyde (NDA) as a derivatization reagent to quantify conversion. This treatment of the deacetylated substrate leads to benzisoindole formation which in turn quenches the fluorescence signal of the aminocoumarin intramolecularly, a strategy that we have used successfully for the development of homogeneous assays for AMC-lysine derivatives before.⁶⁴ Therefore, we investigated the stability and linearity of the fluorescence signal and the general possibility to quench the signal of the deacetylated metabolite by benzisoindole formation in a desired 96 well microplate based assay design (see **Figure S2**).

We observed that the fluorescence of both spermidine derivatives, Ac-spermidine-AMC (**23**) and Spermidine-AMC (**26**), increased in a linear fashion with increasing concentration. Therefore, a four-point dilution (3.5, 5.25, 7.0, 10.5 µM) of both compounds was prepared and

the fluorescence was determined. Linearity (regression coefficient $R^2 = 0.999$) was excellent in both cases (see **Figures S2a+b**). In a follow-up experiment, the enzymatic conversion of Ac-spermidine-AMC was simulated. A dilution of Ac-spermidine-AMC (**23**), complemented to an initial total concentration of 10.5 μM with H₂N-spermidine-AMC (**26**) was prepared. A stable fluorescence signal for all dilution points was observed (see **Figure S2c**). With addition of a NDA containing stop solution the fluorescence signal of H₂N-spermidine-AMC (**26**) was quenched and a linear increasing signal with an increasing concentration of acetylated substrate was monitored (see **Figure S2d, Table S2**).

We designed a high throughput assay set-up as depicted in **Figure 5**. In the first assay step the synthesized substrate (**23**) is deacetylated by HDAC10. For the second step a stop solution containing NDA is added. In presence of a nucleophile (here Mesna) NDA forms a benzoindole structure with primary amines.⁶⁵ As mentioned above the benzoindole intramolecularly quenches the fluorescence signal of the aminocoumarin. This allows for the quantification of the remaining acetylated substrate by measuring the fluorescence signal. HDAC10 inhibitors decrease the deacetylation of the substrate by HDAC10 which leads to an increase of the measured fluorescence signal.

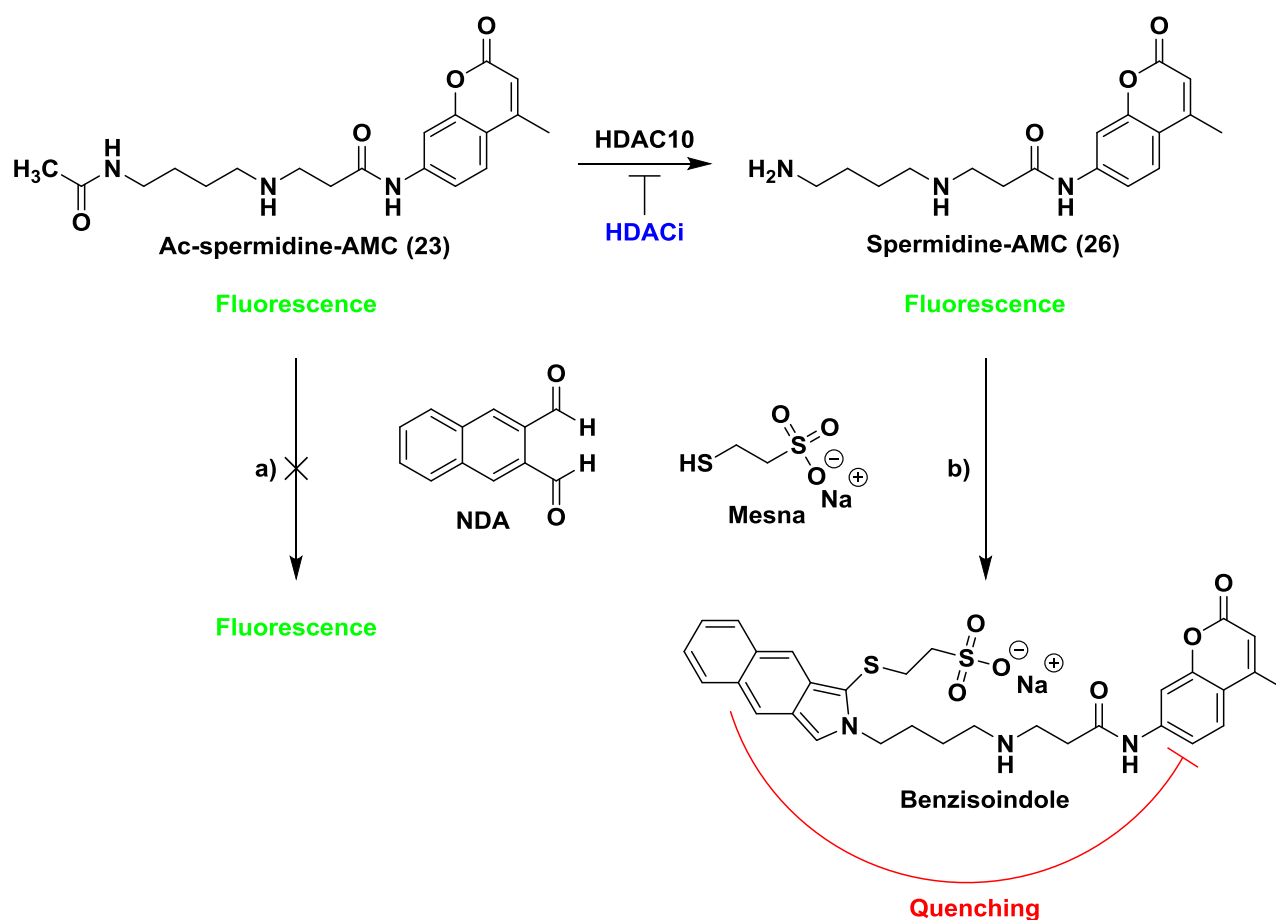


Figure 5: Setup of the homogeneous microplate based assay system. **23** is incubated with drHDAC10. After adding stop solution containing naphthalene-2,3-dialdehyde (NDA) the fluorescence is measured ($\lambda_{\text{ex}} = 330 \text{ nm}$, $\lambda_{\text{em}} = 390 \text{ nm}$): a) Ac-spermidine-AMC is not able to react with NDA; fluorescence is still high at 390 nm; b) Ac-spermidine-AMC is deacetylated by HDAC10; reaction of NDA with Spermidine-AMC in the presence of a nucleophile (here Mesna) leads to formation of a substituted benzisoindeole which quenches the fluorescence at 390 nm intramolecularly. Thus, inhibitors of PDAC activity lead to a high fluorescence signal at 390 nm.

We then determined the robustness of the system in the microplate format. The variability of an assay system can be described by using the Z' -factor which designates the separation band between positive and negative controls. A value between 1 and 0.50 indicates an excellent assay quality.⁶⁶ According to the determined values (Z' -factors ≥ 0.50 , **Table S3**) we demonstrated that our assay is capable of generating robust results.

To demonstrate the measurement of HDAC10 inhibition, we determined the IC₅₀ value of a reported HDAC10 inhibitor. For this purpose, we chose Quisinostat which was recently determined to bind tightly to hHDAC10 with an EC₅₀ of 10 nM in time-resolved fluorescence resonance energy transfer experiments.⁶⁰ Using our new assay substrate Ac-spermidine-AMC (**23**), we measured an IC₅₀ value of 50 ± 5 nM (**Figure 6**). The similarity of the IC₅₀ values determined in our assay and the EC₅₀ values reported from the ligand displacement assay underlines the validity of our assay to measure inhibition of HDAC10.

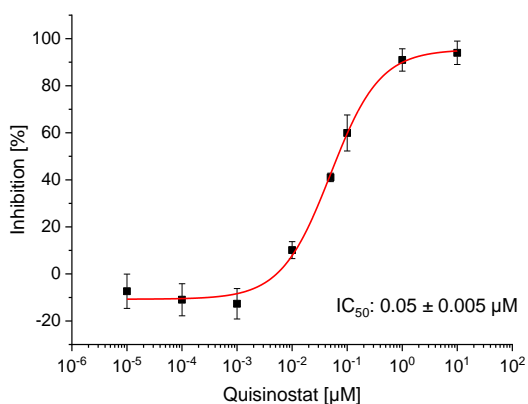
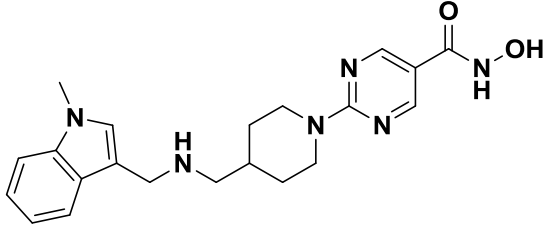


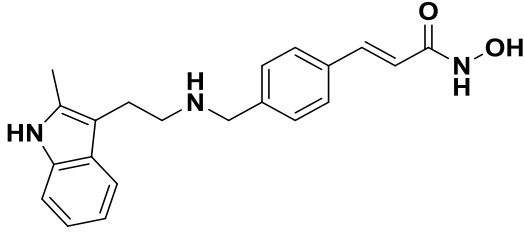
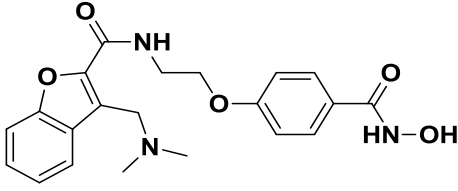
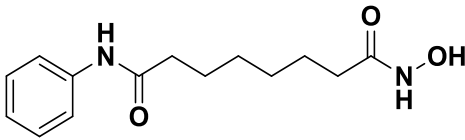
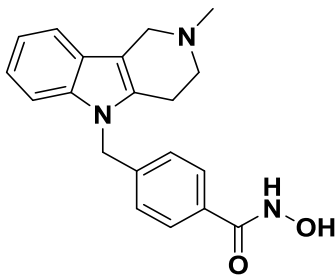
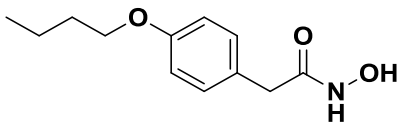
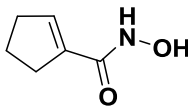
Figure 6. IC₅₀ value of Quisinostat on drHDAC10; one experiment performed in quadruplicate, error bars represent standard deviation of the mean of quadruplicates (error of the IC₅₀ value is shown as SEM of the non-linear regression).

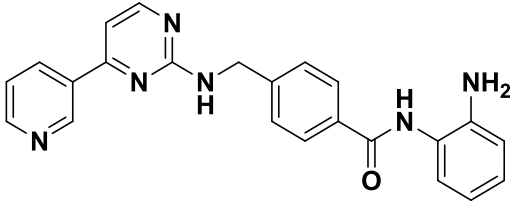
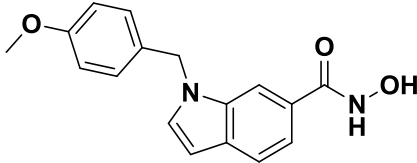
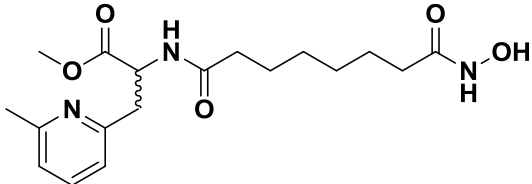
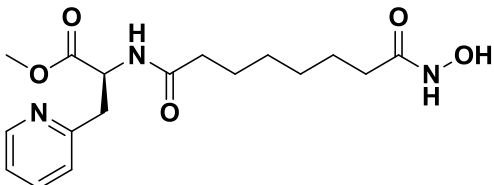
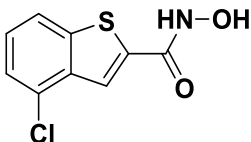
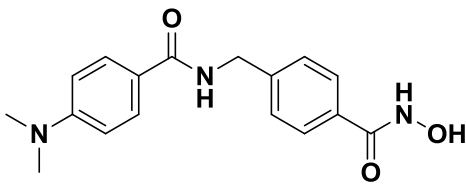
SCREENING FOR HDAC10 INHIBITORS

With a validated assay in hand we tested four sets of compounds for inhibition of HDAC10. The first compound set was compiled from reported HDAC inhibitors (see **Table 1**). It contained unselective inhibitors (Quisinostat (**11**), Panobinostat (**9**), Abexinostat (**12**) and Vorinostat (**6**)), HDAC6-selective inhibitors Tubastatin A (also HDAC10, **14**), Bufexamac (**27**)⁶⁷ and BRD9757 (**28**),⁶⁸ the HDAC8-selective compound PCI-34051 (**29**)⁶⁹ and Mocetinostat (**13**), a class I selective HDAC inhibitor.⁷⁰ We added further compounds from an in-house library to the set (**30-34**). **Table 2** depicts the inhibitory data of cinnamic acid derivatives. This compound class was previously described as inhibitors of hHDAC6 and *Schistosoma mansoni* histone deacetylase 8 (*Sm*HDAC8).⁷¹ Further, a selection of benzhydroxamates was tested (see **Table 3**). Benzhydroxamates were reported as selective HDAC8 inhibitors.⁷² Since for Tubastatin A, a “selective” HDAC6 inhibitor, effects against HDAC10 were shown, a set of oxazole compounds was included which had been reported by us as selective HDAC6 inhibitors (see **Table 4**).⁷³

Table 1. Structures and results of drHDAC10 pretesting of known HDAC inhibitors

Compound	Pretest NDA Assay drHDAC10 % inhibition @ c [μ M]
Quisinostat (11) 	91 % @ 1 60 % @ 0.1 IC ₅₀ : 0.05 ± 0.005 μ M

Panobinostat (9) 	> 95 % @ 1 65 % @ 0.1
Abexinostat (12) 	> 95 % @ 1 45 % @ 0.1
Vorinostat (6) 	43 % @ 1 < 10 % @ 0.1
Tubastatin A (14) 	> 95 % @ 1 82 % @ 0.1
Bufexamac (27) 	64 % @ 1 26 % @ 0.1
BRD9757 (28) 	93 % @ 1 45 % @ 0.1

<p>Mocetinostat (13)</p> 	<p>< 10 % @ 1</p> <p>< 10 % @ 0.1</p>
<p>PCI-34051 (29)</p> 	<p>17 % @ 1</p> <p>14 % @ 0.1</p>
<p>ST70 (30)⁷⁴</p> 	<p>51 % @ 1</p> <p>11 % @ 0.1</p>
<p>ST71 (31)⁷⁴</p> 	<p>64 % @ 1</p> <p>< 10 % @ 0.1</p>
<p>TB5 (32)⁷¹</p> 	<p>56 % @ 1</p> <p>11 % @ 0.1</p>
<p>AW12 (33)⁷⁵</p> 	<p>42 % @ 1</p> <p>< 10 % @ 0.1</p>

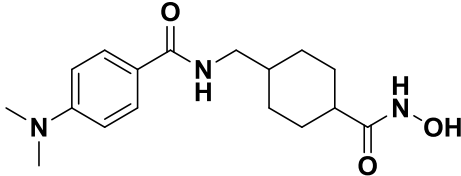
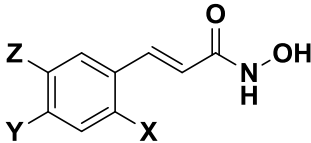
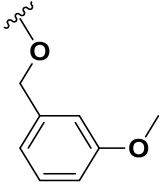
AW19 (34) ⁷⁶	19 % @ 1
	11 % @ 0.1

Table 2. Structures and results of drHDAC10 pretesting of cinnamic acid derivatives

Compound	X	Y	Z	Pretest NDA Assay drHDAC10 % inhibition @ c [μM]
				
TB8 (35a)	-Cl	H	H	73 % @ 1 37 % @ 0.1
TB51 (35b)	-Cl	-Cl	H	> 95 % @ 1 53 % @ 0.1
TB53 (35c)	-Br	-H	-F	50 % @ 1 12 % @ 0.1
TB54 (35d)	-Br	-H	-OCH ₃	39 % @ 1 11 % @ 0.1
TB76 (35e)	-Br	-H	-H	85 % @ 1 23 % @ 0.1
TB77 (35f)	-H	-H	-Cl	69 % @ 1 18 % @ 0.1
TB27 (35g)		-H	-H	24 % @ 1 18 % @ 0.1

TB38 (35h)	-H		-OCH ₃	30 % 17 %	@ 1 @ 0.1
TB73 (36)				54 % < 10 %	@ 1 @ 0.1
TB75 (37)				64 % 46 %	@ 1 @ 0.1

Table 3. Structures and results of drHDAC10 pretesting of benzhydroxamate compounds

Compounds	R	X	Pretest NDA Assay drHDAC10 % inhibition @ c [μM]	
TH65 (38a)		-OCH ₃	< 10 % < 10 %	@ 1 @ 0.1
TH68 (38b)		-OCH ₃	31 % 14 %	@ 1 @ 0.1
TH70 (38c)		-OCH ₃	< 10 % < 10 %	@ 1 @ 0.1

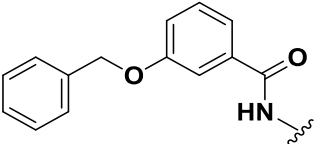
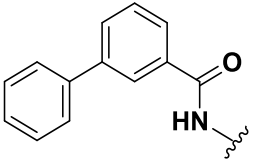
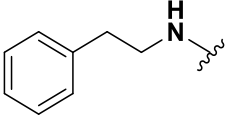
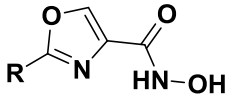
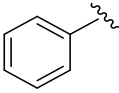
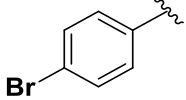
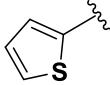
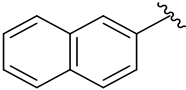
TH77 (38d)		-Cl	20 % 11 %	@ 1 @ 0.1
TH95 (38e)		-OCH ₃	< 10 % < 10 %	@ 1 @ 0.1
TH149 (38f)		-OCH ₃	19 % < 10 %	@ 1 @ 0.1

Table 4. Structures and results of drHDAC10 pretesting of oxazole compounds

Compounds 	R	Pretest NDA Assay drHDAC10 % inhibition @ c [μM]
JS18 (39a)		45 % @ 1 < 10 % @ 0.1
JS28 (39b)		> 95 % @ 1 32.6 % @ 0.1
JS35 (39c)		37 % @ 1 < 10 % @ 0.1
JS41 (39d)		34 % @ 1 < 10 % @ 0.1

All compounds were tested in a first screening at two concentrations (1 and 0.1 μM). For further investigations we set a cut-off of more than 30 % inhibition at 0.1 μM. Besides Quisinostat, four of the unselective inhibitors, three cinnamic acid derivatives and one oxazole

compound exceeded this potency. For these nine hits and Vorinostat as a reference inhibitor IC₅₀ values were determined (**Table 5**, **Figure S3**).

Table 5. IC₅₀ values against HDAC1, 6, 8 and 10 of screening hits

Compound	drHDAC10	HDAC10 binding assay	hHDAC1 (ZMAL)	hHDAC6 (ZMAL)	hHDAC8 (FDL)
Quisinostat (11)	50 ± 5 nM	10 nM*	3 ± 0.3 nM	182 ± 22 nM	64 ± 3 nM
Panobinostat (9)	51 ± 7 nM	2 nM	2 ± 0.1 nM	4 ± 0.4 nM	89 ± 6 nM
Abexinostat (12)	134 ± 26 nM	4 nM*	24 ± 2 nM	9 ± 0.3 nM	820 ± 149 nM
Vorinostat (6)	2000 ± 240 nM	200 nM*	117 ± 6 nM	104 ± 9 nM	400 ± 100 nM
Tubastatin A (14)	30 ± 3 nM	19 nM	1916 ± 420 nM	34 ± 17 nM	1440 ± 120 nM
BRD9757 (28)	147 ± 15 nM	32 nM	4800 ± 1300 nM	455 ± 75 nM	< 10 % @ 100 µM
JS28 (39b)	400 ± 43 nM	34 nM	14470 ± 1100 nM	59 ± 9 nM	14370 ± 2950 nM
TB8 (35a)	185 ± 47 nM	2 nM	1454 ± 470 nM	95 ± 21 nM	54 ± 9 nM
TB51 (35b)	112 ± 19 nM	6 nM	3630 ± 190 nM	710 ± 88 nM	705 ± 120 nM
TB75 (37)	273 ± 58 nM	24 nM	2700 ± 200 nM	225 ± 33 nM	205 ± 32 nM

*from Géraldy et al.⁶⁰

We compared the activity based potency with the recently published HDAC10 binding assay as mentioned above. This assay system was already used to show HDAC10 binding for Tubastatin A, Quisinostat and Abexinostat.⁶⁰ On the one hand we were able to confirm the previously presented binding data for these compounds in our activity based system, on the other

hand we verified the drHDAC10 inhibition by showing a strong hHDAC10 binding for all the other hits (see **Table 5**).

Further, the activity of the hit compounds against hHDAC1, 6 and 8 was measured (see **Table 5**). As expected, a strong effect on HDAC1 as well as HDAC8 was observed for the unselective inhibitors (**6**, **9**, **11**, **12**). For the remaining substances only a moderate to weak inhibition against HDAC1 and 8 was noticed. Only TB8 (**35a**) and TB75 (**37**) stood out with an IC_{50} of 54 nM and 205 nM against HDAC8. However, all compounds showed a strong inhibition of hHDAC6. Since HDAC6 and HDAC10 are both members of class IIb and share a high similarity in their amino acid sequence, this was not surprising. The data also matched the results for the strong HDAC10 binding of the HDAC6 inhibitor Tubastatin A and its derivatives.

We observed that the interaction between a basic part of the molecule and the gatekeeper was not mandatory for HDAC10 inhibition. While many of the most active compounds **9**, **11**, **12** and **14** contain a basic amine which may be able to interact with the gatekeeper, we see strong inhibition for other structures (TB8 (**35a**) and TB51 (**35b**)) without a basic moiety as well. Indeed, TB8 and TB51 gave the strongest binding in the FRET-assay. Vorinostat was presented as a strong HDAC10 binder in the previous studies ($0.2 \mu M^{60}$). In contrast, in our activity assay a weak inhibition with an IC_{50} value of $2 \mu M$ was measured. The discrepancy between the two assay systems could be caused by the use of different enzymes. For the binding assay a recombinant human HDAC10 was used, while zebrafish HDAC10 was applied for the activity assay system. Further, some smaller discrepancies were also noted for other compounds. Overall, a good general agreement between the two different setups was noted. While all identified inhibitors showed binding affinities in a similar range, their inhibitory activities differed stronger. For the compounds with a basic moiety binding affinity and inhibition differed less

than for the others. The cinnamic acid moiety seems to be favorable for HDAC10 inhibition. Besides Panobinostat (**9**), some new HDAC10 inhibitors (TB8 (**35a**), TB51 (**35b**) and TB75 (**37**)) were identified within this set. No hit was identified among our set of simple benzhydroxamate compounds. However, for the more complex compounds Abexinostat and Tubastatin A, both containing a benzhydroxamate moiety, a strong inhibition of HDAC10 was shown. Thus, we conclude that the benzhydroxamate moiety in combination with an appropriate cap group may lead to potent HDAC10 inhibition. The data from the oxazole set demonstrated that it is possible to diverge between HDAC6 and 10 inhibition. JS28 (**39b**) turned out to be a good HDAC10 inhibitor, whereas the other oxazole compounds (**39a**, **39c** and **39d**) had just a moderate inhibitory effect on HDAC10.

In order to rationalize the obtained biochemical data, docking studies were carried out using available crystal structures of drHDAC10 (PDB ID 6UHU)⁷⁷ as well as human HDAC6 (PDB ID 5EDU),⁵⁴ HDAC1 (PDB ID 5ICN)⁷⁸ and HDAC8 (PDB ID 2V5X)⁷⁹ to account for the observed selectivity profile of some hits. Noteworthy, crystal structures of drHDAC6 in complex with hydroxamic acid derivatives have shown that the inhibitors can chelate the catalytic zinc ion in either mono- or bidentate fashion.^{54, 80-83} Hence, two different settings were used for docking of the hits into HDAC6 structure to investigate plausible binding modes.

The pan HDAC inhibitors Abexinostat (**12**), Quisinostat (**11**) and Panobinostat (**9**), which all bear a basic moiety in the capping group, were among the most active compounds tested against HDAC10. The derived docking results, reveal that the capping group of these inhibitors (**Figure 7**) is able to undergo salt bridge interactions between the protonated amine and the gatekeeper residue Glu274⁶⁰ as well as hydrophobic interactions with Phe204 or Trp205. Additionally, the benzhydroxamate moiety shows the classically observed interactions in the lysine binding tunnel

encompassing a bidentate chelation of the zinc ion, three H-bond interactions with His136, His137 and Tyr307 as well as aromatic interactions with residues lining the tunnel.

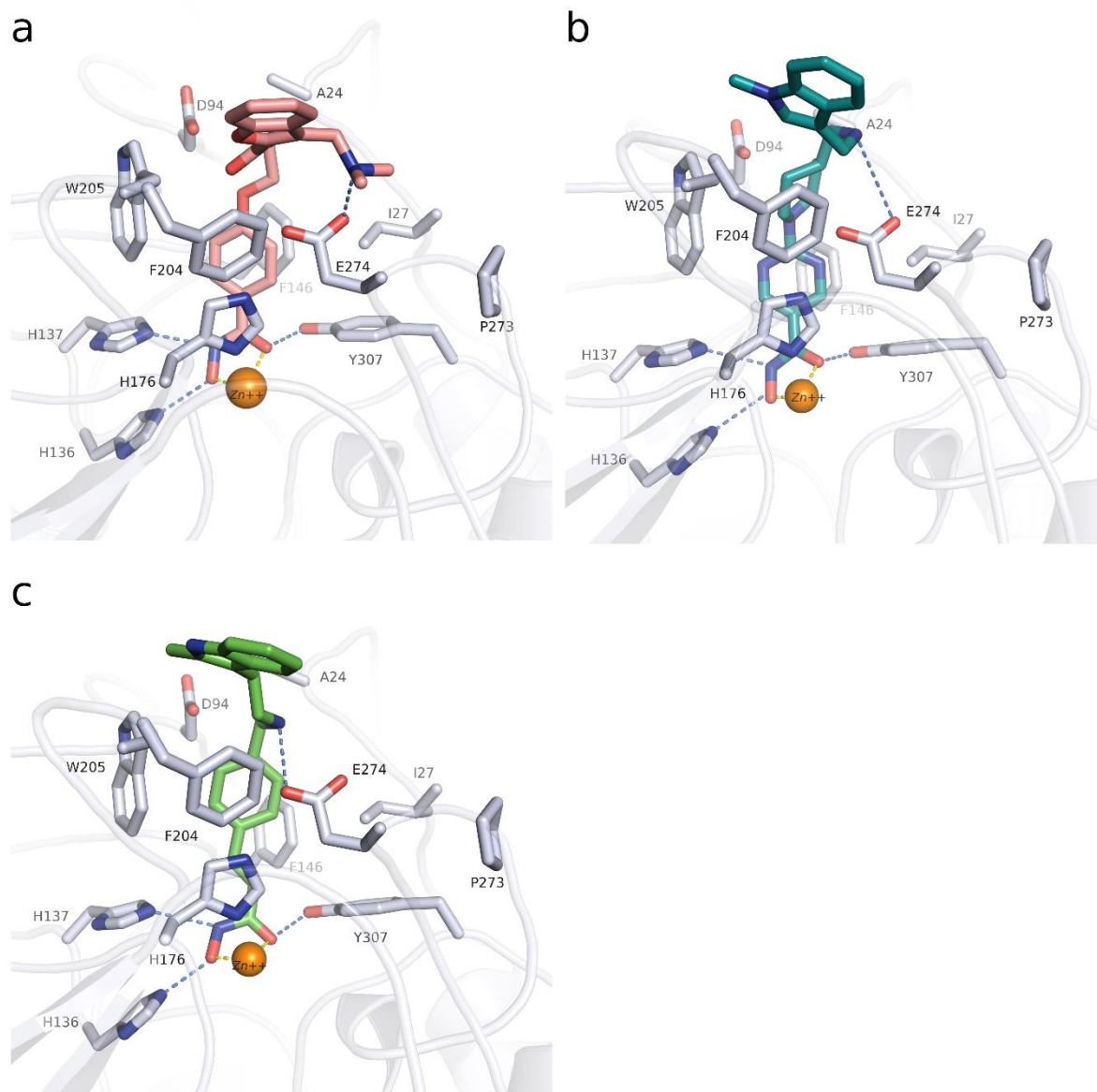


Figure 7. Predicted binding mode in drHDAC10 (PDB ID 6UHU) of pan-inhibitors Abexinostat (**12**), Quisinostat (**11**) and Panobinostat (**9**): a) Abexinostat (colored salmon), b) Quisinostat (colored teal), and c) Panobinostat (colored green). Side chains of binding site residues are shown as white sticks and the catalytic zinc ion as orange spheres. H-bonds and salt bridge interactions are depicted as blue-dashed lines and coordination of the zinc ion by the ligand as yellow-dashed lines.

As previously discussed, several reported potent and “selective” HDAC6 inhibitors also exhibited potent inhibition of HDAC10. This comes as no surprise, since HDAC6 and -10 are the only class IIb HDAC members and share a sequence identity of > 45% (sequence identity of the ligand binding site is around 68%). Tubastatin A (**14**), for instance, showed equal nanomolar potency against HDAC6 and HDAC10 and weak activity against HDAC1 and HDAC8. The derived docking studies in drHDAC10 reveal that, as previously proposed,⁶⁰ the piperidine-NH of Tubastatin A is able to undergo salt bridge interactions with Glu274, while the indole ring shows hydrophobic interactions with Ile27 and Trp205 (**Figure 8a**). In HDAC6, we obtained a docking pose similar to that described in the literature.⁸⁴ Here, Tubastatin A chelates the zinc ion in a monodentate fashion, the phenyl ring of the linker is embedded in the hydrophobic lysine tunnel, while the tetrahydro- γ -carboline moiety is embedded against a hydrophobic patch formed by Phe620, Pro501, His500 and L749 (**Figure 8b**). In the case of HDAC8, although the docking pose displays a bidentate coordination of the zinc ion, the hydrophobic cap group is majorly surface-exposed, which might account for the weak activity of Tubastatin A against HDAC8 (**Figure 8c**). Meanwhile, in the obtained docking pose in HDAC1 no proper chelation of the zinc ion can be observed (**Figure 8d**).

Docking studies offer however little explanation for the selectivity of other previously reported inhibitors towards HDAC6 and -10 e.g. BRD9757 (**28**). As seen in the case of BRD9757, the inhibitor seems to bind almost identically in the different HDAC isoforms and only interacts with residues lining the highly conserved lysine tunnel (**Figure S4**). Here it's important to note that studies have shown that the selectivity of some HDAC6 inhibitors is driven by entropic factors and that the binding of the linker in the lysine tunnel of HDAC6 may be driven by desolvation.⁸⁵⁻

⁸⁶ The binding of BRD9757 to HDAC6 is accompanied by entropic gain, whereas in HDAC8 it's

accompanied by entropic loss.⁸⁵ Hence, the selectivity for the compounds towards HDAC10 over HDAC1 and HDAC8 might also be entropically driven.

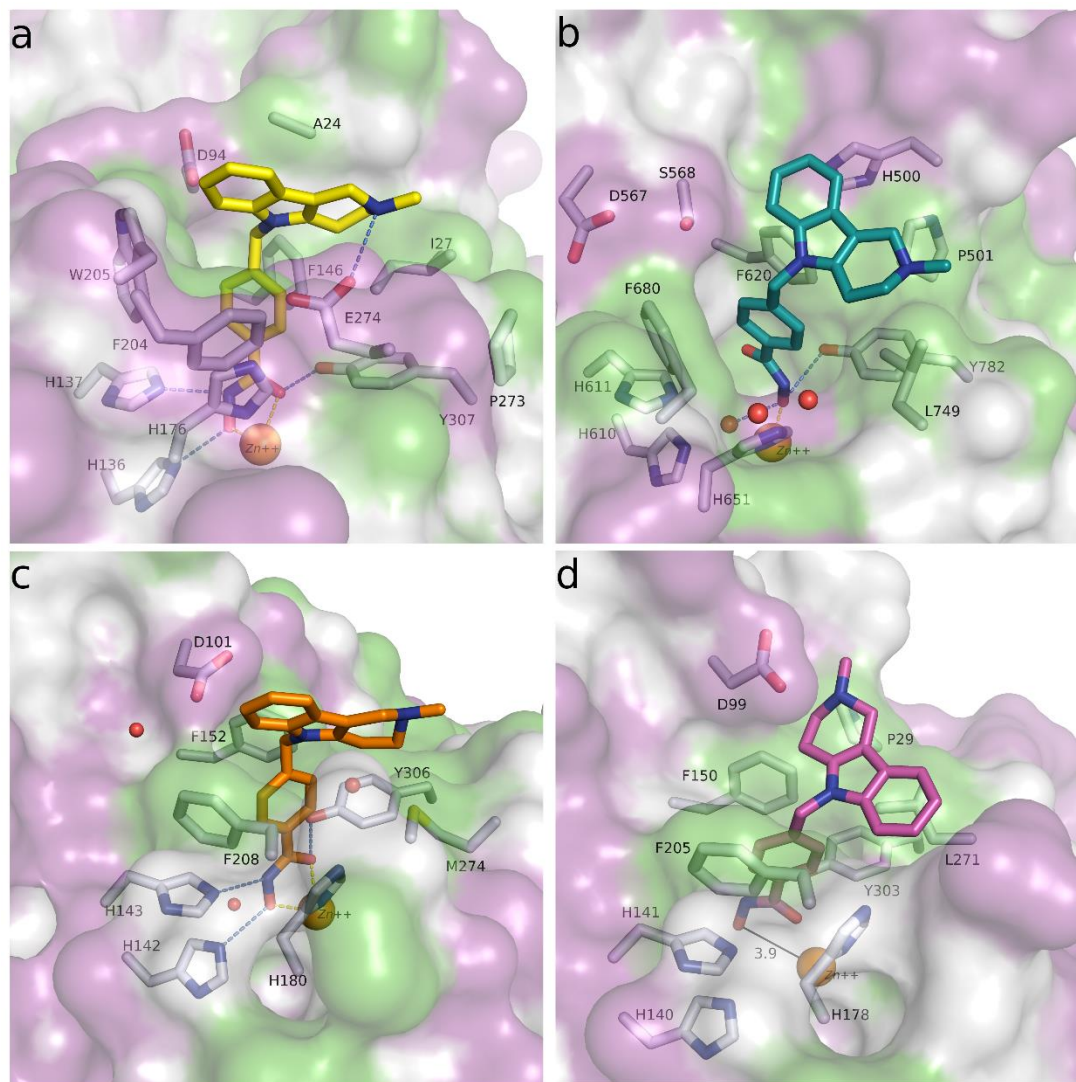


Figure 8. Predicted binding modes of Tubastatin A (**14**) in different HDAC isoforms: a) Tubastatin A (yellow sticks) in drHDAC10 (PDB ID 6UHU), b) Tubastatin A (teal sticks) in HDAC6 (PDB ID 5EDU), c) Tubastatin A (orange sticks) in HDAC8 (PDB ID 2V5X), d) Tubastatin A (magenta sticks) in HDAC1 (PDB ID 5ICN). The surface of the protein is colored according to lipophilicity; green for hydrophobic and magenta for hydrophilic. Side chains of binding site residues are shown as white sticks and the catalytic zinc ion as orange spheres. H-bonds and salt bridge interactions are depicted as blue-dashed lines and coordination of the zinc ion by the ligand as yellow-dashed lines. Distances are shown as black lines.

Regarding the cinnamic acid based derivative TB75 (**37**), docking into drHDAC10 shows that the compound is able to coordinate the zinc ion in a bidentate manner and undergo the three common H-bond interaction with the conserved histidine and tyrosine residues at the bottom of the tunnel. The naphthyl capping group is embedded in the lysine tunnel where it undergoes π - π stacking interactions with Trp205 and Phe146 (**Figure 9a**). A similar binding mode is observed for TB75 in HDAC6 and HDAC8 (**Figure 9b** and **Figure 9c**, respectively). Meanwhile for HDAC1, where TB75 only shows weak inhibitory activity, our docking studies show that the ligand is not able to properly chelate the zinc ion (**Figure 9d**). A similar observation was obtained for the docking of TB8 (**35a**) and TB51 (**35b**) in the various HDAC isoforms, as exemplified in **Figure 10**. In both drHDAC10 and HDAC6, a bidentate coordination of the zinc ion is observed and the chlorophenyl moiety is nicely accommodated in the hydrophobic lysine tunnel (**Figure 10a** and **Figure 10b**, respectively). On the other hand, the bulky linker cannot be properly embedded into the lysine tunnel of HDAC1, hence, no proper chelation of the zinc ion is observed (**Figure 10c**).

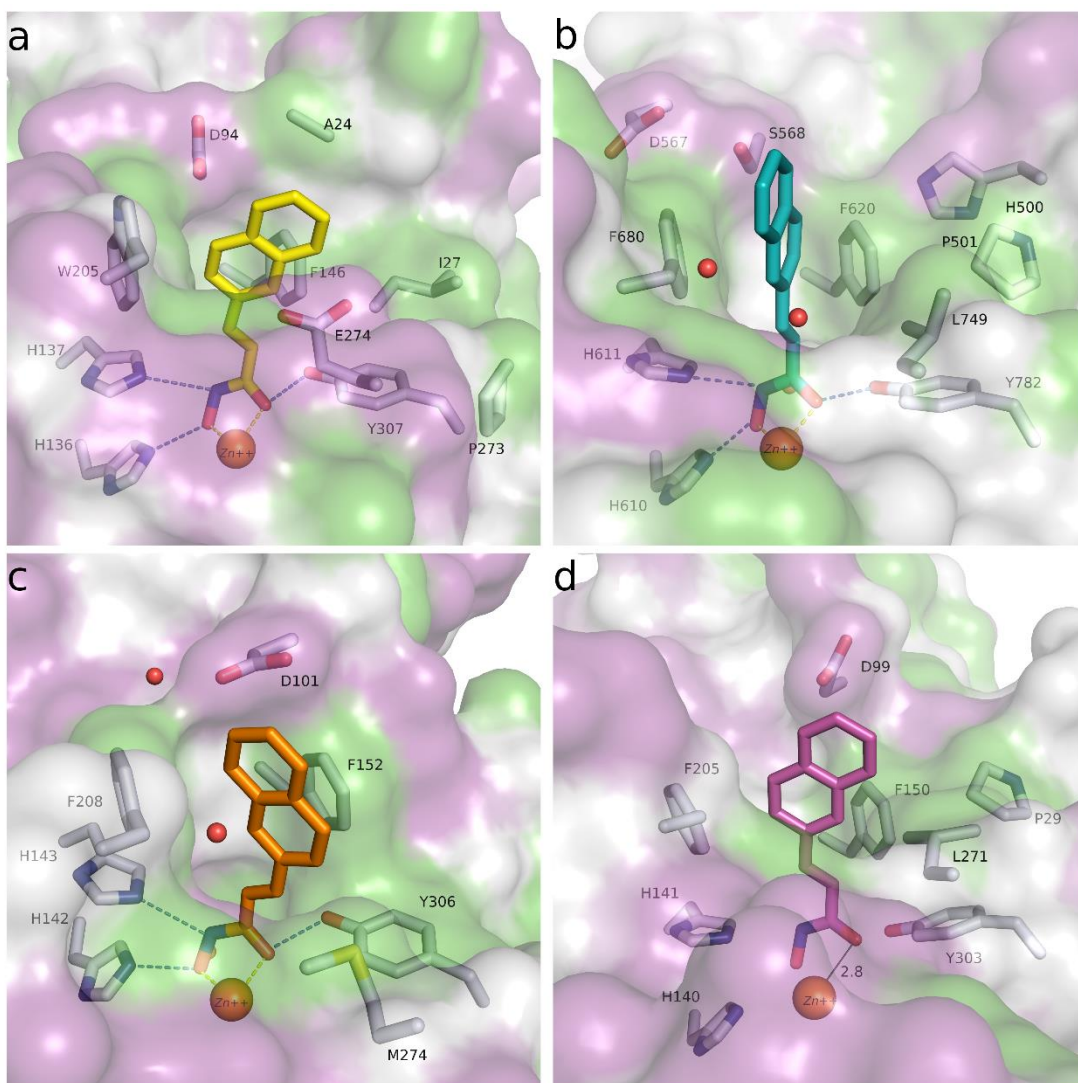


Figure 9. Predicted binding modes of TB75 (37) in different HDAC isoforms: a) TB75 (yellow sticks) in drHDAC10 (PDB ID 6UHU), b) TB75 (teal sticks) in HDAC6 (PDB ID 5EDU), c) TB75 (orange sticks) in HDAC8 (PDB ID 2V5X), d) TB75 (magenta sticks) in HDAC1 (PDB ID 5ICN). The surface of the proteins is colored according to lipophilicity; green for hydrophobic and magenta for hydrophilic. Side chains of binding site residues are shown as white sticks and the catalytic zinc ion as orange spheres. H-bonds and salt bridge interactions are depicted as blue-dashed lines and coordination of the zinc ion by the ligand as yellow-dashed lines. Distances are shown as black lines.

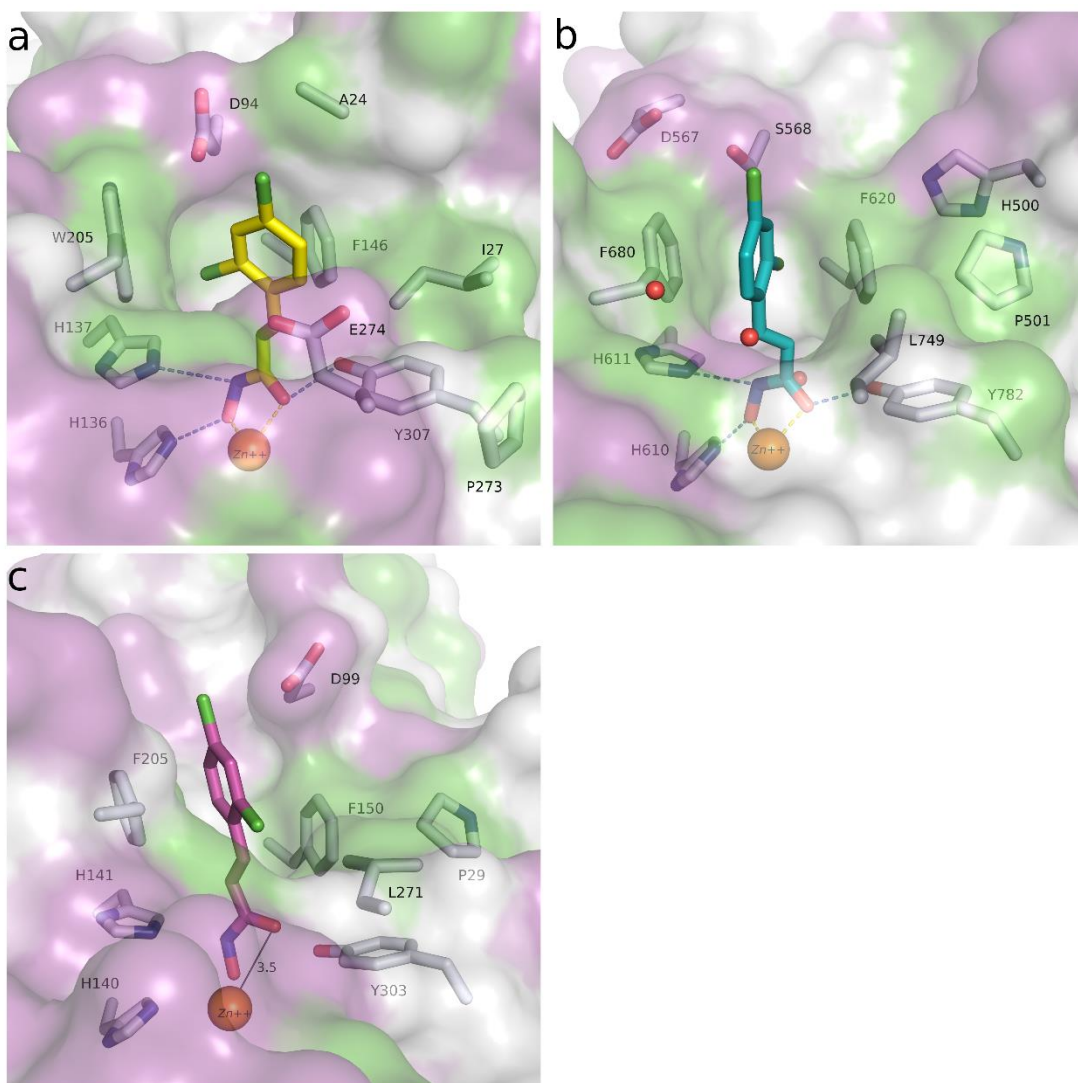


Figure 10: Predicted binding modes of TB51 (**35b**) in different HDAC isoforms: a) TB51 (yellow sticks) in drHDAC10 (PDB ID 6UHU), b) TB51 (teal sticks) in HDAC6 (PDB ID 5EDU), c) TB51 (magenta sticks) in HDAC1 (PDB ID 5ICN). The surface of the proteins is colored according to lipophilicity; green for hydrophobic and magenta for hydrophilic. Side chains of binding site residues are shown as white sticks and the catalytic zinc ion as orange spheres. H-bonds and salt bridge interactions are depicted as blue-dashed lines and coordination of the zinc ion by the ligand as yellow-dashed lines. Distances are shown as black lines.

In summary, the obtained docking results can partly explain the experimentally observed inhibitory activity and selectivity profile of the herein reported hits. Nevertheless, one has to bear in mind that entropic factors also play essential roles in the binding of the ligands. Regarding

benzhydroxamate derivatives, bulky capping groups at the *p*-position can be well accommodated in the binding cleft of both HDAC6 and HDAC10 and usually results in selectivity against other HDAC subtypes. A basic moiety in the capping group which is able to undergo salt bridge interaction with the gatekeeper Glu274 seems to be not essential for HDAC10 inhibition, albeit it might be a driving factor for an increase in potency. Due to the high homology between HDAC6 and -10, the task of designing purely selective HDAC10 inhibitors might prove difficult but already examples from the oxazole series showed that selective inhibition for HDAC6 over HDAC10 can be achieved.

However, *m*-substituted benzhydroxamate derivatives, previously reported as selective HDAC8 inhibitors,^{72, 87-88} were proven to show little inhibitory activity against HDAC10. The docking studies clearly show that the *m*-substitution pattern is not suitable for binding to HDAC10. In the obtained docking poses we observe clashes between the *p*-substituent (-OCH₃ or -Cl) and Trp205/Asp94 as well as electrostatic clashes between the capping phenyl group and the gatekeeper Glu274 (**Figure S5**).

On the other hand, cinnamic acid derivatives seem to represent good starting points for the development of HDAC10 inhibitors; bulkier groups like *o*-chlorophenyl and naphthyl moieties are still well accommodated in the lysine tunnel and the mouth of the active site cleft. These bulky groups are less suitable for binding to HDAC1, which leads to selectivity over this HDAC isoform. Further modifications of the capping group can be exploited to develop more potent and selective inhibitors.

Further, screening hits were also investigated in a cellular LysoTracker-Assay in neuroblastoma cells. Oehme et al. showed that doxorubicin treatment in a neuroblastoma cell model induces

autophagic flux as a major resistance mechanism. The control of lysosomal activity was linked to HDAC10 activity. HDAC10 inhibition as well as its depletion induced accumulation of lysosomes, which also affected autophagy and sensitized for drug-induced cell death. So HDAC10 was identified as a promising target in advanced stage 4 neuroblastoma.³³ HDAC10 inhibitor mediated accumulation of lysosomes is detected by the LysoTracker-Assay. This assay system allows us to determine cellular effects of our HDAC10 inhibitors.³⁴

We studied the impact of our screening hits on the accumulation of lysosomes in neuroblastoma cells. Accumulation was monitored by fluorescence microscopy and quantified via flow cytometry analysis. Via fluorescence microscopy an increase of the LysoTracker signal was monitored for all of our hits (see **Figure 11**). While for JS28 (**39b**) and BRD9757 (**28**) high concentrations were necessary to get a signal, a significant increase of the accumulation of lysosomes at moderate concentrations (1.0 - 7.5 μ M) was observed for the rest of the hits. For the highly potent and unselective inhibitors Quisinostat (**11**), Panobinostat (**9**) and Abexinostat (**12**) extraordinary strong response was monitored. Tubacin as selective HDAC6 inhibitor was included as negative control compound.⁸⁹ No influence of HDAC6 inhibition on the accumulation of lysosomes was seen.

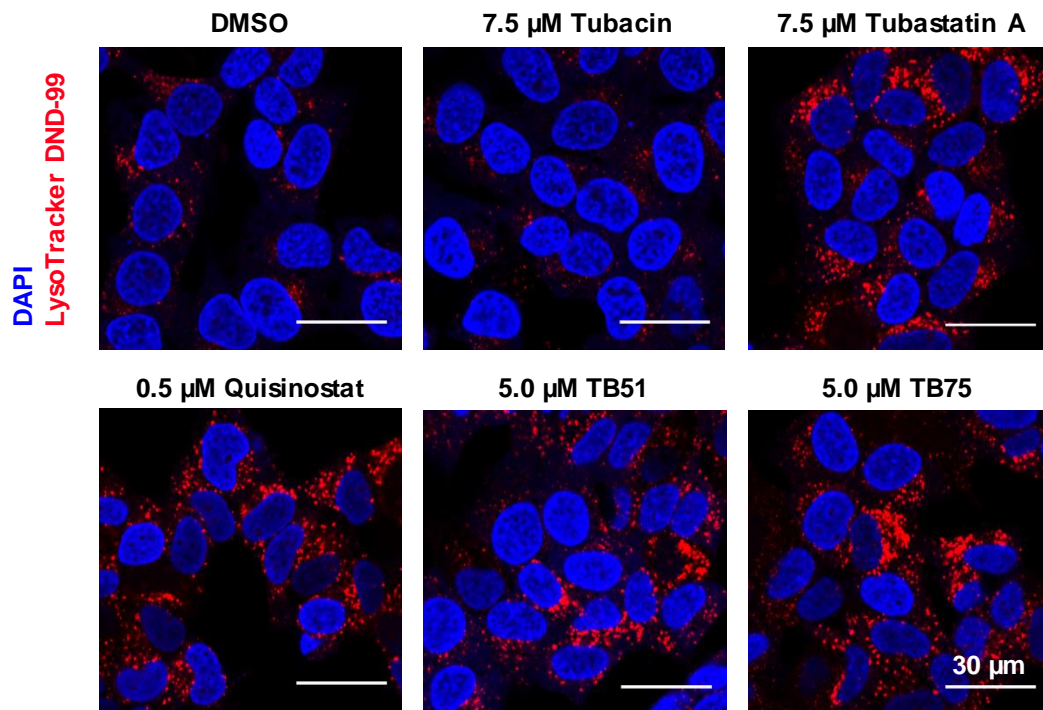


Figure 11. Fluorescence microscopy analysis of LysoTracker DND-99 staining 24 h after treatment with 7.5 μM Tubacin (HDAC6i), 7.5 μM Tubastatin A (**14**), 0.5 μM Quisinostat (**11**), 5 μM TB51 (**35b**) and 5.0 μM TB75 (**37**). Nuclei were stained with DAPI (4',6-Diamidino-2-phenylindole).

Quantification via flow cytometry confirmed the tendency of fluorescence microscopy analysis (see **Table 7**). LysoTracker fluorescence was normalized against DMSO control. For Tubacin (7.5 μM) a 1.1-fold change of the LysoTracker signal was detected. Effects of BRD9757 (**28**) and JS28 (**39b**) were in the same range (1.2-1.3 @ 20 μM). The majority of the HDAC10 inhibitors (**6**, **14**, **35a**, **35b**, **37**) showed a significant effect between 1.5- and 2.0-fold increase. Under treatment with unselective inhibitors (**9**, **11** and **12**) occurred already at nanomolar concentrations a strong increase of the measured signal up to 3-fold. While for HDAC class IIb inhibitors a weak signal was observed, selective HDAC6 inhibition did not result in a significant LysoTracker signal. The more pronounced the HDAC class I activity of the compounds is, the higher is the accumulation of lysosomes in neuroblastoma cells. These observations match the

data from previous experiments³⁴ and we conclude, that HDAC10 inhibition and lysosome accumulation show a good correlation. However, inhibition of HDAC class I seems also to be involved in accumulation and shows a strong synergistic effect with HDAC10 inhibition.

Table 6. Quantification of accumulation of lysosomes

Compound	Tested concentration	LysoTracker effect
Quisinostat (11) n=3	0.5 μ M	3.0 \pm 0.65
Panobinostat (9) 0.01 μ M n=2 0.004 μ M n=6	0.01 μ M	2.0 \pm 0.15
	0.004 μ M	1.5 \pm 0.2
Abexinostat (12) ³⁴ n=5	0.1 μ M	1.7 \pm 0.23
Vorinostat (6) n=2	1 μ M	2.0 \pm 0.03
Tubastatin A (14) ³⁴ n=4	7.5 μ M	1.6 \pm 0.08
BRD9757 (28) n=3	20.0 μ M	1.3 \pm 0.07
JS28 (39b) n=3	20.0 μ M	1.2 \pm 0.07
TB8 (35a) n=3	5.0 μ M	1.5 \pm 0.24
TB51 (35b) n=3	5.0 μ M	2.0 \pm 0.27
TB75 (37) n=3	5.0 μ M	1.7 \pm 0.04
Tubacin ³⁴ n=4	7.5 μ M	1.1 \pm 0.07

Table 7. The LysoTracker effect indicates the fold-change of the fluorescence signal of the neuroblastoma cells. The fluorescence signal is proportional to the amount of lysosomes within the cells.

CONCLUSION

We designed and synthesized the first fluorescent polyamine substrate for HDAC10 which can be used in a validated conversion assay suitable for high-throughput screening.

By screening a set of HDAC inhibitors, the assay confirmed reported potent HDAC10 binders as strong HDAC10 inhibitors. Furthermore, we used the assay system to identify new HDAC10 inhibitors. It turned out that inhibition of HDAC10 tends to correlate with HDAC6 inhibition, whereas HDAC1 and HDAC8 inhibition was not associated in our set with activity on HDAC10. Among hydroxamates, a strong affinity to HDAC1 and 8 does not exclude HDAC10 inhibition, as exemplified by the unselective inhibitors **9**, **11**, and **12** but the HDAC8 selective inhibitor PCI-34051 did not inhibit HDAC10. We tested Mocetinostat, a benzamide HDAC inhibitor, which is described as class I selective agent, as well and did not see any effects on HDAC10. The selectivity profiles of the compounds were rationalized by docking studies. Some of our compounds identified as potent HDAC10 inhibitors showed promising effects on inhibiting lysosome activity in neuroblastoma cells. These compounds are useful tools for further investigation of the impact of HDAC10 in tumor cells and for increasing our understanding of HDAC10 as a potential drug target.

To gain a good selectivity for HDAC10 over HDAC6 will be a big challenge for prospective compound design. This will be necessary to develop selective probes and drugs and our novel assay system will be a powerful enabling tool in this endeavor.

EXPERIMENTAL SECTION

Chemistry

Starting materials and reagents were purchased from different suppliers. No further purification was done. For R_f -determination thin-layer plates from Merck (TLC Silica gel 60 F₂₅₄ and TLC Silica gel 60 RP-18 F_{254s}) were used and analyzed under UV light (254 nm). Mass spectrometry (MS) was performed on Advion expression CMS spectrometer using a APCI ion source or ESI. Spectra for final compounds were recorded with high resolution mass spectrometry (HRMS) on Exactive device (Thermo Fisher Scientific) operating in ESI mode. Theoretical masses were calculated with Biological Magnetic Resonance Data Bank (www.bmrb.wisc.edu). ¹H NMR and ¹³C NMR spectra were recorded on Bruker Avance III HD spectrometer at 400 and 100 MHz by using the signal of the deuterated solvent as internal standard. Following abbreviation were used to report the spectra: ¹H: chemical shift δ (ppm), multiplicity (s = singlet, d = doublet, dd = doublet of doublets, t = triplet, q = quartet, m = multiplet, b = broad), integration, coupling constant (J in Hz). ¹³C, chemical shift δ (ppm). HMBC and HSQC experiments were applied for the assignment. The purity of the final compounds (>95 %) was determined by HPLC and UV detection (λ = 210 nm). HPLC analysis was performed using the following conditions: Eluent A, H₂O containing 0.05 % TFA; Eluent B, acetonitrile containing 0.05 % TFA, flow rate 1 mL/min, linear gradient conditions (0–4 min, A = 90 %, B = 10 %; 4–29 min, linear increase to 100 % of B; 29–31 min, B = 100 %; 31–40 min, A = 10 %, B = 90 %), Phenomenex Kinetex 5 μ m XB- C 18 (100 Å, 250x4.60 mm).

tert-Butyl (3-((4-methyl-2-oxo-2H-chromen-7-yl)amino)-3-oxopropyl)carbamate (18).

Boc- β -alanine (1778 mg, 9.40 mmol, 1.5 eq) and BOP-Cl (2635 mg, 10.35 mmol, 1.7 eq) were

suspended in dry DCM (15 ml). After adding triethylamine (1903 mg, 18.81 mmol, 3.0 eq) and stirring for 30 min at room temperature 7-Amino-4-methylcoumarin (1098 mg, 6.27 mmol, 1.0 eq) was added. Reaction was stirred overnight at room temperature. After removing solvent under reduced pressure, water was added and pH < 5 was adjusted with HCl (2 M). Suspension was extracted with DCM. Organic layers were dried over magnesium sulfate, filtrated and solvent was removed. Crude product was purified via flash column chromatography (DCM/MeOH). Yield, 68 % of a white solid. R_f 0.58 (DCM/MeOH 95:5 (v/v)). ^1H NMR (DMSO- d_6 , δ [ppm]): 10.38 (s, 1H, CO-NH-AMC), 7.77 (d, J = 2.0 Hz, 1H, AMC H8), 7.71 (d, J = 8.4 Hz, 1H, AMC H5), 7.48 (dd, J = 8.4, 2.0 Hz, 1H, AMC H6), 6.92 (t, J = 5.6 Hz, 1H, CO-NH-CH₂), 6.27 – 6.25 (m, 1H, AMC H3), 3.27 – 3.20 (m, 2H, NH-CH₂-CH₂-CO), 2.56 – 2.50 (overlapping with DMSO signal, m, 2H, HN-CH₂-CH₂-CO), 2.40 (d, J = 1.2 Hz, 3H, CH₃), 1.38 (s, 9H, (CH₃)₃-CH₂-O). ^{13}C NMR (DMSO- d_6 , δ [ppm]): 170.64 (CH₂-CO-NH), 160.47 (CO-AMC), 155.98 (Boc-CO-NH), 154.08 (AMC C9), 153.55 (AMC C4), 142.92 (AMC C7), 126.31 (AMC C5), 115.50 (AMC C6), 115.27 (AMC C10), 112.58 (AMC C3), 105.91 (AMC C8), 78.07 ((CH₃)₃-CH₂-O), 37.33 (NH-CH₂-CH₂-CO), 36.70 (HN-CH₂-CH₂-CO), 28.65 ((CH₃)₃-CH₂-), 18.40 (CH₃). MS (APCI, +): 346.2 [M+H]⁺.

3-Amino-N-(4-methyl-2-oxo-2H-chromen-7-yl)propanamide (19). **18** (1487 mg, 4.30 mmol, 1.0 eq) was solved in DCM (10 ml). Trifluoroacetic acid (4903 mg, 43.00 mmol, 10.0 eq) and triethylsilane (5000 mg, 43.00 mmol, 10.0 eq) were added and the mixture was stirred for 2 h at 40 °C. Solvent was removed under reduced pressure. Residue was suspended via ultrasonification in 5 ml ethyl acetate. After adding 5 ml cyclohexane and cooling on ice the suspension was filtrated and washed with a solvent mixture (EE/CH, 50/50, 0 °C). Precipitation was dried and use without further purification. Yield, 95 % of a white solid. R_f 0.40

(DCM/MeOH 95:5 (v/v)). ^1H NMR (DMSO- d_6 , δ [ppm]): 10.63 (s, 1H, CO-NH-AMC), 7.85 – 7.77 (m, 4H, $^+\text{H}_3\text{N}$ -CH₂ + AMC H8), 7.75 (d, J = 8.4 Hz, 1H, AMC H5), 7.47 (dd, J = 8.4, 2.0 Hz, 1H, AMC H6), 6.30 – 6.27 (m, 1H, AMC H3), 3.17 – 3.07 (m, 2H, $^+\text{H}_3\text{N}$ -CH₂-CH₂-CO), 2.77 (t, J = 6.6 Hz, 2H, $^+\text{H}_3\text{N}$ -CH₂-CH₂-CO), 2.41 (d, J = 1.2 Hz, 3H, CH₃). ^{13}C NMR (DMSO- d_6 , δ [ppm]): 169.58 (HN-CO-CH₂), 160.42 (CO-AMC), 158.50 + 158.19 (TFA) 154.08 (AMC C9), 153.54 (AMC C4), 142.56 (AMC C7), 126.46 (AMC C5), 115.52 (AMC C6 + C10), 112.77 (AMC C3), 106.04 (AMC C8), 35.09 ($^+\text{H}_3\text{N}$ -CH₂-CH₂-CO), 33.87 ($^+\text{H}_3\text{N}$ -CH₂-CH₂-CO), 18.40 (CH₃). MS (APCI, +): 247.2 [M+H]⁺.

N-(4-methyl-2-oxo-2H-chromen-7-yl)-3-((2-nitrophenyl)sulfonamido)propanamide (20).
19 (728 mg, 2.02 mmol, 1.0 eq) and 2-Nitrobenzenesulfonyl chloride (535 mg, 2.42 mmol, 1.2 eq) were dissolved in THF (10 ml, 0 °C). After adding triethylamine (818 mg, 8.08 mmol, 4.0 eq) the reaction was stirred for 30 min at room temperature. Reaction mixture (white flakes) was filtrated and washed with a solvent mixture (EE/CH, 75/25, 15 ml, 0 °C). Precipitation was dried and use without further purification. Yield, 100 % of a white solid. R_f , 0.47 (EE/CH 75/25 (v/v)). ^1H NMR (DMSO- d_6 , δ [ppm]): 10.41 (s, 1H, CO-NH-AMC), 8.24 (t, J = 5.6 Hz, 1H, SO₂-NH-CH₂), 8.06 – 8.01 (m, 1H, Nosyl H6), 8.00 – 7.95 (m, 1H, Nosyl H3), 7.90 – 7.83 (m, 2H, Nosyl H4,5), 7.74 – 7.69 (m, 2H, AMC H5,8), 7.44 (dd, J = 8.8, 2.0 Hz, 1H, AMC H6), 6.28 – 6.25 (m, 1H, AMC H3), 3.27 – 3.20 (m, 2H, HN-CH₂-CH₂-CO), 2.62 (t, J = 6.8 Hz, 2H, HN-CH₂-CH₂-CO), 2.40 (d, J = 1.2 Hz, 3H, CH₃). ^{13}C NMR (DMSO- d_6 , δ [ppm]): 169.90 (HN-CO-CH₂), 160.46 (CO-AMC), 154.05 (AMC C9), 153.54 (AMC C4), 148.19 (Nosyl C2), 142.71 (AMC C7), 134.47 (Nosyl C4), 133.11 (Nosyl C5), 132.94 (Nosyl C1), 129.91 (Nosyl C6), 126.33 (AMC C5), 124.85 (Nosyl C3), 115.51 (AMC C6), 115.37 (AMC C10), 112.65 (AMC C3),

105.96 (AMC C8), 39.13 (HN-CH₂-CH₂-CO), 37.03 (HN-CH₂-CH₂-CO), 18.40 (CH₃). MS (APCI, +): 432.2 [M+H]⁺.

N-(4-bromobutyl)acetamide (21). 4-Bromobutene-1-amine hydrobromide (529 mg, 2.29 mmol, 1.0 eq) was suspended in dry THF (10 ml). Acetylchloride (1786 mg, 22.9 mmol, 10.0 eq) and cesium carbonate (2985 mg, 9.16 mmol, 4.0 eq) were added. After stirring the reaction for 5 h at 60 °C, the solvent was removed and water was added. Aqueous mixture was extracted with DCM. Organic layers were dried over magnesium sulfate, filtrated and solvent was removed. Crude product was purified via flash column chromatography (DCM/MeOH). Yield, 64 % of a colorless oil. R_f 0.49 (DCM/MeOH 95:5 (v/v)). ¹H NMR (DMSO-d₆, δ [ppm]): 7.86 (bs, 1H, CH₂-NH-CO), 3.54 (t, J = 6.8 Hz, 2H, Br-CH₂-CH₂), 3.08 - 2.99 (m, 2H, CH₂-CH₂-NH), 1.84 – 1.72 (m, 5H, -CH₃ + Br-CH₂-CH₂-CH₂), 1.55 – 1.44 (m, 2H, -CH₂-CH₂-CH₂-NH). ¹³C NMR (DMSO-d₆, δ [ppm]): 169.45 (-COCH₃), 37.91 (CH₂-CH₂-NH), 35.30 (Br-CH₂-), 30.15 (-CH₂-CH₂-CH₂-NH), 28.24 Br-CH₂-CH₂-CH₂), 23.00 (-CH₃). MS (APCI, +): 194.1 + 196.1 [M+H]⁺.

3-((N-(4-acetamidobutyl)-2-nitrophenyl)sulfonamido)-N-(4-methyl-2-oxo-2H-chromen-7-yl)propanamide (22). **20** (147 mg, 0.34 mmol, 1.0 eq), N-(4-bromobutyl)acetamide (**21**) (132 mg, 0.68 mmol, 2.0 eq), potassium carbonate (71 mg, 0.51 mmol, 1.5 eq) and potassium iodide (11 mg, 0.07 mmol, 0.2 eq) were suspended in DMF (5 ml). Reaction mixture was stirred at 45 °C for 4 h and overnight at room temperature. Solvent was removed under reduced pressure. Crude product was purified via flash column chromatography (DCM/MeOH). Yield, 48 % of a colorless oil. R_f 0.63 (DCM/MeOH 90/10 (v/v)). ¹H NMR (DMSO-d₆, δ [ppm]): 10.45 (s, 1H, CO-NH-AMC), 8.06 – 8.02 (m, 1H, Nosyl H₆), 7.99 – 7.95 (m, 1H, Nosyl H₃), 7.91 – 7.80 (m, 3H, Nosyl H_{4,5} + CH₂-NH-CO), 7.74 – 7.70 (m, 2H, AMC H_{5,8}), 7.43 (dd, J = 8.8, 2.0 Hz, 1H, AMC H₆), 6.28 – 6.26 (m, 1H, AMC H₃), 3.63 – 3.56 (m, 2H, N-CH₂-CH₂-CO), 3.34 – 3.28 (m,

2H, Nosyl-N-CH₂-CH₂-CH₂), 3.04 – 2.96 (m, 2H, CH₂-CH₂-NH-CO), 2.73 – 2.66 (m, 2H, N-CH₂-CH₂-CO), 2.40 (d, J = 1.2 Hz, 3H, AMC CH₃), 1.78 (s, 3H, CO-CH₃), 1.58 – 1.56 (m, 2H, CH₂-CH₂-NH-CO), 1.40 – 1.29 (m, 2H, Nosyl-N-CH₂-CH₂-CH₂). ¹³C NMR (DMSO-d₆, δ [ppm]): 169.89 (CH₂-CO-NH), 169.41 (HN-CO-CH₃), 160.44 (AMC CO), 154.05 (AMC C9), 153.53 (AMC C4), 148.00 (Nosyl C2), 142.61 (AMC C7), 134.92 (Nosyl C4), 132.95 (Nosyl C5), 132.07 (Nosyl C1), 130.15 (Nosyl C6), 126.38 (AMC C5), 124.76 (Nosyl C3), 115.49 (AMC C6), 115.42 (AMC C10), 112.68 (AMC C3), 105.94 (AMC C8), 48.18 (Nosyl-N-CH₂-CH₂-CH₂), 43.89 (Nosyl-N-CH₂-CH₂-CO), 38.39 (CH₂-CH₂-NH-CO), 36.42 (Nosyl-N-CH₂-CH₂-CO), 26.66 (Nosyl-N-CH₂-CH₂-CH₂), 25.79 (CH₂-CH₂-NH-CO), 23.01 (NH-CO-CH₃), 18.40 (AMC CH₃). MS (APCI, +): 545.2 [M+H]⁺.

3-((4-Acetamidobutyl)amino)-N-(4-methyl-2-oxo-2H-chromen-7-yl)propanamide (23). 22
 (34 mg, 0.06 mmol, 1.0 eq) and potassium carbonate (17 mg, 0.13 mmol, 2.0 eq) were solved in MeCN (5 ml). After adding thiophenol (10 mg, 0.09 mmol, 1.5 eq) the reaction mixture was stirred for 4 h at 35 °C. Solvent was removed and crude product was purified via flash column chromatography (H₂O/MeCN + 0.1 % TFA). Yield, 53 % of a white solid. R_f, 0.30 (H₂O/MeCN 50/50 (v/v) + 0.05 % TFA). ¹H NMR (DMSO-d₆, δ [ppm]): 10.65 (s, 1H, CO-NH-AMC), 8.48 (b s, 2H, CH₂-NH₂⁺-CH₂), 7.90 (t, J = 5.6 Hz, 1H, CONH-CH₂-CH₂), 7.80 (d, J = 2.0 Hz, 1H, AMC H8), 7.75 (d, J = 8.4 Hz, 1H, AMC H5), 7.48 (dd, J = 8.4, 2.0 Hz, 1H, AMC H6), 6.31 - 6.27 (m, 1H, AMC H3), 3.28 – 3.18 (m, 2H, CH₂-CH₂-CO), 3.06 (q, 6.8 Hz, 2H, CONH-CH₂-CH₂-CH₂-NH₂⁺), 3.01 - 2.92 (m, 2H, CONH-CH₂-CH₂-CH₂-CH₂-NH₂⁺), 2.83 (t, J = 6.8 Hz, 2H, CH₂-CH₂-CO), 2.41 (d, J = 1.2 Hz, 3H, AMC CH₃), 1.81 (s, 3H, CO-CH₃), 1.65 – 1.55 (m, 2H, CONH-CH₂-CH₂-CH₂-CH₂-NH₂⁺), 1.49 - 1.39 (m, 2H, m, 2H, CONH-CH₂-CH₂-CH₂-NH₂⁺). ¹³C NMR (DMSO-d₆, δ [ppm]): 169.53 (H₃C-CO-NH), 169.30 (CH₂-CH₂-CONH),

160.41 (AMC C2), 159.04 – 157.81 (TFA), 154.08 (AMC C10), 153.53 (AMC C4), 142.52 (AMC C7), 126.48 (AMC C5), 115.55 (AMC C6 + C9), 112.80 (AMC C3), 106.05 (AMC C8), 47.18 (CONH-CH₂-CH₂-CH₂-CH₂-NH₂⁺), 42.76 (CH₂-CH₂-CO), 38.21 (CONH-CH₂-CH₂-CH₂-CH₂-NH₂⁺), 32.77 (CH₂-CH₂-CO), 26.71 (CONH-CH₂-CH₂-CH₂-CH₂-NH₂⁺), 23.40 (CONH-CH₂-CH₂-CH₂-CH₂-NH₂⁺), 23.04 (COCH₃), 18.40 (AMC CH₃). HRMS (ESI, +): 360.1914 [M+H]⁺. Calculated mass: 360.1923 [M+H]⁺. Purity: 97% (11.50 min).

tert-Butyl (4-((N-(3-((4-methyl-2-oxo-2H-chromen-7-yl)amino)-3-oxopropyl)-2-nitrophenyl)sulfonamido)butyl)carbamate (24). **20** (200 mg, 0.47 mmol, 1.0 eq), 4-(Bocamino)butylbromide (141 mg, 0.56 mmol, 1.2 eq), potassium carbonate (96 mg, 0.70 mmol, 1.5 eq) and potassium iodide (15 mg, 0.09 mmol, 0.2 eq) were suspended in DMF (5 ml). Reaction mixture was stirred at 45 °C for 4 h and overnight at room temperature. Solvent was removed under reduced pressure. Crude product was purified via flash column chromatography (DCM/MeOH). Yield, 31 % of a colorless solid. R_f, 0.59 (EE/CH 75/25 (v/v)). ¹H NMR (DMSO-d₆, δ [ppm]): 10.45 (s, 1H, CO-NH-AMC), 8.06 – 8.02 (m, 1H, Nosyl H6), 7.99 – 7.95 (m, 1H, Nosyl H3), 7.91 – 7.81 (m, 2H, Nosyl H4,5), 7.74 – 7.69 (m, 2H, AMC H5,8), 7.43 (dd, J = 8.0, 2.0 Hz, 1H, AMC H6), 6.83 (t, J = 5.5 Hz, 1H, CH₂-NH-Boc), 6.27 (d, J = 1.2 Hz, 1H, AMC H3), 3.63 – 3.56 (m, 2H, N-CH₂-CH₂-CO), 3.33 – 3.26 (m, 2H, Nosyl-N-CH₂-CH₂-CH₂), 2.93 – 2.83 (m, 2H, CH₂-CH₂-NH-Boc), 2.74 – 2.66 (m, 2H, N-CH₂-CH₂-CO), 2.40 (d, J = 1.2 Hz, 3H, AMC CH₃), 1.57 – 1.45 (m, 2H, CH₂-CH₂-NH-Boc), 1.36 (s, 9H, (CH₃)₃-C-O), 1.34 – 1.28 (m, 2H, Nosyl-N-CH₂-CH₂-CH₂). ¹³C NMR (DMSO-d₆, δ [ppm]): 169.87 (CH₂-CO-NH), 160.44 (AMC CO), 156.01 (Boc-CO), 154.05 (AMC C9), 153.53 (AMC C4), 147.99 (Nosyl C2), 142.61 (AMC C7), 134.91 (Nosyl C4), 132.95 (Nosyl C5), 132.09 (Nosyl C1), 130.14 (Nosyl C6), 126.38 (AMC C5), 124.76 (Nosyl C3), 115.49 (AMC C6), 115.42 (AMC C10),

112.68 (AMC C3), 105.93 (AMC C8), 77.82 ((CH₃)₃-C-O), 48.17 (Nosyl-N-CH₂-CH₂-CH₂), 43.85 (N-CH₂-CH₂-CO), 39.84 (CH₂-NH-Boc (HMBC)), 36.39 (N-CH₂-CH₂-CO), 28.65 ((CH₃)₃-C-O), 27.04 (Nosyl-N-CH₂-CH₂-CH₂), 25.73 (CH₂-CH₂-NH-Boc), 18.40 (AMC CH₃). MS (ESI, +): 624.9 [M+Na]⁺.

3-((N-(4-aminobutyl)-2-nitrophenyl)sulfonamido)-N-(4-methyl-2-oxo-2H-chromen-7-yl)propanamide (25). **24** (138 mg, 0.23 mmol, 1.0 eq) was solved in DCM (5 ml).

Trifluoroacetic acid (392 mg, 3.44 mmol, 15.0 eq) and triethylsilane (266 mg, 2.29 mmol, 10.0 eq) were added and the mixture was stirred for 2 h at 40 °C. Solvent was removed under reduced pressure. Crude product was purified via flash column chromatography (DCM/MeOH). Yield, 86 % of a colorless oil. R_f 0.38 (DCM/MeOH 90/10 (v/v)). ¹H NMR (DMSO-d₆, δ [ppm]): 10.53 (s, 1H, CO-NH-AMC), 8.07 - 8.03 (m, 1H, Nosyl H6), 8.00 - 7.96 (m, 1H, Nosyl H3), 7.92 - 7.82 (m, 2H, Nosyl H4,5), 7.75 - 7.70 (m, 2H, AMC H5,8), 7.51 - 7.37 (m, 4H, AMC H6 + NH₃⁺), 6.28 (d, J = 1.2 Hz, 1H, AMC H3), 3.65 - 3.58 (m, 2H, N-CH₂-CH₂-CO), 3.41 - 3.27 (overlapping with H₂O-Peak, m, 2H, Nosyl-N-CH₂-CH₂-CH₂), 2.82 - 2.74 (m, 2H, CH₂-CH₂-NH₃⁺), 2.73 - 2.66 (m, 2H, N-CH₂-CH₂-CO), 2.40 (d, J = 1.2 Hz, 3H, AMC CH₃), 1.67 - 1.56 (m, 2H, CH₂-CH₂-NH₃⁺), 1.56 - 1.45 (m, 2H, Nosyl-N-CH₂-CH₂-CH₂). ¹³C NMR (DMSO-d₆, δ [ppm]): 169.93 (CH₂-CO-NH), 160.45 (AMC CO), 158.37 + 158.06 (TFA), 154.05 (AMC C9), 153.54 (AMC C4), 148.01 (Nosyl C2), 142.61 (AMC C7), 134.99 (Nosyl C4), 133.00 (Nosyl C5), 131.99 (Nosyl C1), 130.14 (Nosyl C6), 126.38 (AMC C5), 124.80 (Nosyl C3), 115.49 (AMC C6), 115.43 (AMC C10), 112.69 (AMC C3), 105.94 (AMC C8), 47.97 (Nosyl-N-CH₂-CH₂-CH₂), 43.83 (N-CH₂-CH₂-CO), 39.04 (CH₂-CH₂-NH₃⁺), 36.27 (N-CH₂-CH₂-CO), 25.31 (CH₂-CH₂-NH₃⁺), 24.96 (Nosyl-N-CH₂-CH₂-CH₂), 18.41 (AMC CH₃). MS (APCI, +): 503.2 [M+H]⁺.

3-((4-Aminobutyl)amino)-N-(4-methyl-2-oxo-2H-chromen-7-yl)propanamide (26). 25

(122 mg, 0.20 mmol, 1.0 eq) and potassium carbonate (109 mg, 0.79 mmol, 4.0 eq) were solved in MeCN (8 ml). After adding thiophenol (65 mg, 0.59 mmol, 3.0 eq) the reaction mixture was stirred for 4 h at 35 °C. Crude product was purified via flash column chromatography (H₂O/MeCN + 0.1 % TFA). Yield, 80 % of a yellow solid. R_f, 0.50 (H₂O/MeCN 50/50 (v/v) + 0.1 % TFA). ¹H NMR (DMSO-d₆, δ [ppm]): 10.70 (s, 1H, CO-NH-AMC), 8.64 (bs, 2H, CH₂-NH₂⁺-CH₂), 7.92 – 7.77 (m, 4H, ⁺H₃N-CH₂ + AMC H8), 7.75 (d, J = 8.8 Hz, 1H, AMC H5), 7.47 (dd, J = 8.8, 2.0 Hz, 1H, AMC H6), 6.29 (d, J = 1.2 Hz, 1H, AMC H3), 3.29 – 3.19 (m, 2H, ⁺H₂N-CH₂-CH₂-CO), 3.05 - 2.93 (m, 2H, ⁺H₃N-CH₂-CH₂-CH₂-CH₂-NH₂⁺), 2.89 – 2.77 (m, 4H, ⁺H₃N-CH₂-CH₂-CH₂-CH₂-NH₂⁺ + CH₂-CO), 2.41 (d, J = 1.2 Hz, 3H, AMC CH₃), 1.71 – 1.53 (m, 4H, ⁺H₃N-CH₂-CH₂-CH₂-CH₂-NH₂⁺). ¹³C NMR (DMSO-d₆, δ [ppm]): 169.35 (CH₂-CO-NH), 160.42 (AMC CO), 158.63 + 158.32 (TFA), 154.07 (AMC C9), 153.55 (AMC C4), 142.52 (AMC C7), 126.48 (AMC C5), 115.55 (AMC C6 + C10), 112.80 (AMC C3), 106.05 (AMC C8), 46.74 (⁺H₃N-CH₂-CH₂-CH₂-CH₂-NH₂⁺), 42.70 (CH₂-CH₂-CO), 38.65 (⁺H₃N-CH₂-CH₂-CH₂-CH₂-NH₂⁺), 32.74 (⁺H₂N-CH₂-CH₂-CO), 24.59 (⁺H₃N-CH₂-CH₂-CH₂-CH₂-NH₂⁺), 22.87 (⁺H₃N-CH₂-CH₂-CH₂-CH₂-NH₂⁺), 18.41 (AMC CH₃). HRMS (ESI, m/z): 318.1810 [M+H]⁺. Calculated mass: 318.1818 [M+H]⁺. Purity: 99% (10.51 min).

Protein expression

HDAC10 from *Danio rerio* (zebrafish) (residues 2-676) was prepared and purified as previously described¹⁰ with minor modifications. Briefly, protein was expressed in *E. coli* BL21 (DE3) (Agilent) cells in 2x YT media in the presence of 50 µg/mL kanamycin (Gold Bio). Expression was induced when OD₆₀₀ reached 1.0 by addition of 150 µM isopropyl β-D-1-thiogalactopyranoside (IPTG, Gold Bio) and 500 µM ZnSO₄ (Fisher Scientific), and cell cultures

were grown for an additional 18–22 hours at 16 °C. Cells were harvested by centrifugation at 6,000 g and resuspended in lysis buffer containing 50 mM 4-(2-hydroxyethyl)-1-piperazineethanesulfonic acid (HEPES) (pH 8.0), 300 mM NaCl, 2 mM tris-(2-carboxyethyl) phosphine (TCEP), 10% glycerol (v/v), 10 μ M ZnCl₂, 30 mM imidazole, 2 mini-protease inhibitor tablets (Roche), 0.5 mg/mL hen egg-white lysozyme (MilliporeSigma), and 0.1 mg/mL DNaseI (MilliporeSigma). Cells were lysed by sonication and lysate was cleared by centrifugation at 26,000g for 1 hour at 4 °C. The supernatant was loaded onto a 5-mL pre-packed His trap (Ni²⁺) affinity column (GE Healthcare Life Sciences) and HDAC10 was eluted with buffer containing 50 mM HEPES (pH 8.0), 300 mM NaCl, 2 mM TCEP, 10% glycerol (v/v), 10 μ M ZnCl₂, and 500 mM imidazole.

Peak fractions were incubated with Tobacco Etch Virus (TEV) protease and extensively dialyzed overnight at 4 °C against a buffer containing 50 mM HEPES (pH 8.0), 300 mM NaCl, 2 mM TCEP, 10% glycerol (v/v), 10 μ M ZnCl₂, and 30 mM imidazole. The free zebrafish HDAC10 protein was separated from free His-MBP tag by loading the dialyzed protein sample onto a 5-mL pre-packed His trap (Ni²⁺) affinity column (GE Healthcare Life Sciences) and then passing the His trap column flow-through fraction over a column containing amylose resin (NEB Biolabs). The flow-through sample from the amylose column was then loaded onto a HiLoad Superdex S200 (26/600) size exclusion column (GE Healthcare Life Sciences) pre-equilibrated with a buffer containing 50 mM HEPES (pH 7.5), 300 mM KCl, 1 mM TCEP and 5% glycerol (v/v). Protein was concentrated to 2–8 mg/mL, flash-cooled in liquid nitrogen, and stored at -80 °C for further use.

Proof of substrate conversion by HPLC

For the calibration curve stock solutions of Ac-spermidine-AMC [200 μ M] and Spermidine-AMC [200 μ M] in buffer (20 mM Na₂HPO₄, pH 7.9, 10 mM NaCl, 0.25 mM EDTA) were prepared. Fluorescamine solution [600 μ M] was prepared in acetonitrile. Ac-spermidine-AMC and Spermidine-AMC stocks solutions were mixed in nine different mixing ratios to get 50 μ L solution (see **Table S1**). Substrate-metabolite-mixtures were complemented with 50 μ L of fluorescamine solution. Different samples were analyzed via HPLC (Gradient see Chemistry, 5 μ L injected, Phenomenex Kinetex column, UV absorption 210 nm).

Stock solutions of Ac-spermidine-AMC [240 μ M] and Spermidine-AMC [240 μ M] in buffer (20 mM Na₂HPO₄, pH 7.9, 10 mM NaCl, 0.25 mM EDTA) were prepared to proof the substrate conversion by drHDAC10. Fluorescamine solution [600 μ M] was confected in acetonitrile. The enzyme was diluted with buffer to a final concentration of 0.027 mg/mL.

Samples were prepared in eppendorf tubes; each containing 50 μ L auf Ac-spermidine-AMC solution and 10 μ L of enzyme solution. The tubes were incubated at 37 °C for 0-60 min. Reaction was stopped at several time points (0, 10, 15, 20, 30, 45, 60 min) by adding fluorescamine solution, mixing and centrifugation (5 min, 20000 rpm). For time point 0 min stop solution was added before enzyme solution. Supernatant was analyzed by HPLC (see calibration curve, n=1).

Z'-factor

Following equation was used to calculate the Z' value: $Z' = 1 - (3\sigma_{c+} + 3\sigma_{c-})/|\mu_{c+} - \mu_{c-}|$. The standard deviation of the positive control (σ_{c+}) is represented by relative fluorescence units of

conversion by enzyme (buffer, enzyme solution, DMSO, substrate), for standard deviation of the negative control (σ_c) the relative fluorescence units of no substrate conversion was used (buffer, DMSO, substrate). It was shown that there is no significant difference between no substrate conversion (buffer, DMSO) and 100 % inhibition (buffer, enzyme solution, 10 μ M Quisinostat, substrate). μ_{c+} and μ_{c-} are the mean of positive control (no inhibition) and negative control (no conversion of substrate).

Determination was performed on three different days each with 35 values for positive control and 35 values for negative control.

In Vitro Testing

hHDAC1/6

Commercial available human recombinant HDAC1 (BPS Bioscience, catalog no. 50051) and human recombinant HDAC6 (BPS Bioscience, catalog no. 50006) were used. Activity assays were performed in OptiPlate™-96 F black microplates (PerkinElmer). Total assay volume of 60 μ L contains 52 μ L of enzyme solution in incubation buffer (50 mM Tris-HCl, pH 8.0, 137 mM NaCl, 2.7 mM KCl, 1 mM MgCl₂, and 1 mg/mL bovine serum albumin), 3 μ L of increasing concentrations of inhibitors in DMSO and 5 μ L of the fluorogenic substrate ZMAL (Z-(Ac)Lys-AMC) (126 μ M). After incubation step (90 min, 37 °C) 60 μ L of stop solution, containing 5 μ L Trichostatin A (TSA) (33 μ M) and 10 μ L trypsin (6 mg/mL) in trypsin buffer (Tris-HCl 50 mM, pH 8.0, NaCl 100 mM), were added and the plate was incubated for 30 min at 37 °C.

Fluorescence signal was measured on a BMG LABTECH POLARstar OPTIMA plate reader (BMG Labtechnologies, Germany) with an excitation wavelength of 390 nm and an emission wavelength of 460 nm.⁹⁰

hHDAC8

For HDAC8 activity testing commercial available Fluor de Lys (FDL) drug discovery kit (BML-KI178) was used. Enzyme was obtained from cooperation partners (Romier).⁹¹ Assay was performed according to the manufacturer's instructions. Enzyme solution (15 μ L), increasing inhibitor concentrations (10 μ L) and FDL substrate solution (25 μ L) were incubated for 90 min at 37 °C in ½ AreaPlate-96 F microplates (PerkinElmer). Developer solution (50 μ L) was added and the assay was incubated for 45 min at 30 °C. Fluorescence signal was determined as mentioned for HDAC1/6.

HDAC10

All stock solutions were prepared in DMSO; Quisinostat (1 mM), NDA (16 mM) and Ac-spermidine-AMC (10 mM). Compounds for testing were solved and diluted to 12-fold higher than test concentration in DMSO. Ac-spermidine-AMC stock solutions was diluted with assay buffer (20 mM Na₂HPO₄, pH 7.9, 100 mM NaCl, 0.25 mM EDTA, 10 % (v/v) glycerol, 10 mM Mesna, 0.01 % TWEEN 20) to 126 μ M. For assay determination stop solution was prepared, containing 5 μ L NDA (16 mM), 5 μ L Quisinostat (1 mM) and 190 μ L borat buffer (100 mM boric acid, pH 9.5) per well. Directly before using enzyme solution (0.0054 mg/ml) was prepared in assay buffer.

The assay was performed in black 96-well plates (PerkinElmer, OptiPlate™-96 F). Assay buffer was presented in the plate, 55 μ L for the blank, 45 μ L for the blank containing enzyme solution, 50 μ L for the negative control and 40 μ L for the positive control and test compounds. 5 μ L of DMSO were added to the wells of blanks, positive and negative control. Corresponding to the DMSO 5 μ L of increasing concentrations of inhibitors in DMSO were added to the relevant

wells. After adding 10 μ L of enzyme solution (12 nM final assay concentration) to blank containing enzyme, positive control and test compounds, 5 μ L Ac-spermidine-AMC solution (10.5 μ M final assay concentration) were added to negative control, positive control and test compounds. The plate was incubated for 25 min at 25 °C. Before measuring fluorescence (POLARstar plate reader, λ_{ex} = 330 nm, λ_{em} = 390 nm) each well was filled with 200 μ L stop solution.

IC₅₀ calculation

Inhibition was measured at increasing concentration and IC₅₀ was calculated by nonlinear regression with Origin 9.0G software.

FRET Assay

The FRET-assay was performed in white 384-well ProxiPlates (PerkinElmer). Reagents were diluted in assay buffer (50 mM HEPES pH 8.0, 150 mM NaCl, 10 mM MgCl₂, 1 mM EGTA, 0.01% Brij-35). Final assay volume (10 μ L) contains 3 nM GST-HDAC10 (Life Technologies), 30 nM Tubastatin-Alexa647-Tracer (Géraldy et al.⁶⁰), and 0.5 nM LanthaScreen Eu-anti-GST (Life Technologies). Compound stocks (10 mM DMSO) were diluted in assay buffer. An 11-fold 1:3-serial dilution of test compounds (1 μ L) were presented in the plate and complemented by 9 μ L of assay-mix. After incubation (1 h, r.t.) TR-FRET was measured with EnVision plate reader (Ex: 3 flashes of the TRF-europiumlaser; Em: 620 and 665 nm (665/620 nm ratio). Inhibition was calculated by using negative control (2 % DMSO) and positive control (20 μ M Vorinostat). Dose-response curves were fitted in ActivityBase (IDBS) using a four-parameter logistic model and IC₅₀-values were calculated.⁶⁰

Cellular Testing (Fluorescence microscopic and flow cytometric analysis of LysoTracker®

Red staining)

Analysis of LysoTracker staining via confocal fluorescence microscopy or flow cytometry was performed after overnight treatment of SK-N-BE(2)-C cells as described previously.³⁴

Computational Methods

Molecular Docking

The ligands and protein–ligand complexes used herein were prepared using a similar method as reported in our previous published paper.⁸⁷

Ligand Preparation

MOE⁹² (version 2014.09, Chemical Computing Group, Montreal, Canada) was used to generate the molecular structures of all compounds.

The ligands were prepared for docking using the LigPrep tool⁵⁴ as implemented in Schrödinger's software (version 2018-1), where all possible tautomeric forms, as well as stereoisomers, were generated. They were subsequently energy minimized using the integrated Optimized Potentials for Liquid Simulations (OPLS_2005) force field.⁹³ 64 conformers of prepared ligands were calculated with ConfGen using the default settings.^{80, 94}

Protein Preparation

The crystal structures of HDAC10 (drHDAC10; PDB ID: 6UHU), HDAC1 (hsHDAC1; PDB ID: 5ICN), HDAC6 (hsHDAC6; PDB ID: 5EDU) and HDAC8 (hsHDAC8; PDB ID: 2V5X) were downloaded from the Protein Databank (PDB; www.rcsb.org).⁹⁵ With the exception of water

molecules occupying the catalytic pockets that were used for the docking procedures. Further preparations of the protein structures were done using the Protein Preparation Wizard of Schrödinger software.^{82, 96} Bond orders were assigned and hydrogen atoms added, and the H-bond network was subsequently optimized. The protonation states at pH 7.0 were predicted using the Epik-tool in Schrödinger.^{84, 97} The structures were finally subjected to a restrained energy minimization step (rmsd of the atom displacement for terminating the minimization was 0.3 Å) using the OPLS2005 force field.⁹³

Docking in HDAC6 with monodentate chelation: The co-crystallized ligand and three water molecules (HOH921, HOH999 and HOH1011) from PDB ID 5EF7 were retrieved and inserted into the herein used crystal structure of HDAC6 (PDB ID 5EDU) prior the protein preparation and minimization steps mentioned above.

Docking in HDAC6 with bidentate chelation: three water molecules (HOH1015, HOH1006 and HOH1083) were retrieved from PDB ID 6CSQ were retrieved and inserted into the herein used crystal structure of HDAC6 (PDB ID 5EDU) prior the protein preparation and minimization steps mentioned above.

Docking to HDACs

A docking protocol using Glide⁵⁴ was developed and validated by redocking the cocrystallized HDAC inhibitors with the corresponding crystal structure.

Docking studies were done using Glide.^{54, 98-99} The receptor grid preparation for the docking procedure was carried out by assigning the co-crystallized ligand as the centroid of the grid box. The generated 3D conformers of the ligands (refer to Section 3.1.1) were docked into the receptor grid using Glide^{54, 98-99} and the Standard Precision (SP) mode as the scoring function. A total of

20 poses per ligand conformer were included in the post-docking minimization step, and a maximum of 2 docking poses was generated for each ligand conformer.

PAINS Analysis

All tested compounds were checked for structural features which could interfere with the assay system. Screening against PAINS was performed by using PAINS-Remover.¹⁰⁰ All compounds passed the filter.

ASSOCIATED CONTENT

Supporting Information. Additional data on compound purity/identity by HPLC and NMR, assay validation and IC₅₀-determinations, molecular modelling (including pdb-files of docked complexes, molecular string data file.

AUTHOR INFORMATION

Corresponding Author

***Phone:** +497612034896. **Fax:** +497612036321. **E-mail:** manfred.jung@pharmazie.uni-freiburg.de.

Present Addresses

S.A.S.: Department of Biology, The College of New Jersey, 2000 Pennington Road, Ewing, NJ 08618 USA

ORCID IDs:

Aubry K. Miller: 0000-0002-1761-4143

Ina Oehme: 0000-0002-0827-2356

Johannes Ridinger: 0000-0003-1341-7721

Manfred Jung: 0000-0002-6361-7716

Wolfgang Sippl: 0000-0002-5985-9261

Author Contributions

Daniel Herp: Substrate synthesis, assay design and validation, *in vitro* testing of HDAC10, preparation of manuscript.

Johannes Ridinger: Performing LysoTracker-Assay (FACS and confocal microscopy).

Dina Roba: Computational methods, preparation of manuscript.

Stephen A. Shinsky: Expression and purification of drHDAC10.

Karin Schmidtkunz: *In vitro* testing of HDAC1, 6 and 8.

Talha Z. Yesiloglu: Carried out the docking studies.

Theresa Bayer: Synthesis of some of the HDAC inhibitors and provided material for biological testing.

Peter Sehr: Development of FRET-HDAC10 assay and testing of selected inhibitors.

Nikolas Gunkel: Coordination of FRET-HDAC10 testing.

Aubry K. Miller: Coordination of the FRET-HDAC10 assay, preparation of manuscript.

Ina Oehme: Supervision of cellular experiments, preparation of manuscript.

David Christianson: Coordination of HDAC10 expression, preparation of manuscript.

Wolfgang Sippl: Supervision of molecular modelling, preparation of manuscript.

Manfred Jung: Design of study, preparation of manuscript.

The manuscript was written through contributions of all authors. All authors have given approval to the final version of the manuscript.

ACKNOWLEDGMENT

We thank the Deutsche Forschungsgesellschaft (DFG, MJ (Ju295/13-1), WS (Si868/13-1), IO (Oe542/2-1) and INST 39/931-1 for cofinancing of the NMR console) for funding. The work of IO and JR was supported by the H.W.&J. Hector foundation (Grant reference number: M91). Thanks to the National Institute of Health (NIH) for funding DWC (GM49758) and SAS (F32GM125141). Further, we thank Raphael Steimbach for measuring Panobinostat in the FRET-HDAC10 assay.

ABBREVIATIONS

AMC, aminocoumarin; APCI, atmospheric pressure chemical ionization; BOP-Cl, Bis(2-oxo-3-oxazolidinyl)phosphinic chloride; BRET, bioluminescence energy transfer; c, concentration; CH, cyclohexane; DAPI, 4',6-Diamidino-2-phenylindole; DCM, dichloromethane; DMF, dimethylformamide; DMSO, dimethyl sulfoxide; EC₅₀, half maximal effective concentration; EDTA, ethylenediaminetetraacetic acid; EE, ethyl acetate; EGTA, Ethylene glycol-bis(β-aminoethyl ether)-*N,N,N',N'*-tetraacetic acid; ERRα, estrogen-related receptor alpha; ESI, electrospray ionization; Et₃N, triethylamine; Et₃SiH, triethylsilane; eq, equivalent; FDA, Food and Drug Administration; FDL, Fluor de Lys; HDACi(s), histone deacetylase inhibitor(s); HDACs, histone deacetylases; (h)/(z)HDAC10, (human)/(zebrafish) histone deacetylase 10; HMBC, Heteronuclear Multiple Bond Correlation; HPLC, High-performance liquid chromatography; HRMS, high resolution mass spectrometry; HSP90, heat shock protein 90; HSQC, Heteronuclear Single Quantum Coherence; IC₅₀, half maximal inhibitory concentration; KDACs, lysine deacetylase(s); LC-MS, liquid chromatography–mass spectrometry; MeCN, acetonitrile; MeOH, methanol; min, minute; NAD⁺, Nicotinamide adenine dinucleotide; NDA, naphthalene-2,3-dialdehyde; NMR, nuclear magnetic resonance; p53, tumor suppressor p53; rpm, revolutions per minute; PDAC, polyamine deacetylase; r.t., room temperature; Sirt, sirtuin; SMC3, structural maintenance of chromosomes protein 3; *SmHDAC8*, *Schistosoma mansoni* histone deacetylase 8; TFA, trifluoroacetic acid; THF, tetrahydrofuran; TLC, Thin Layer Chromatography; TR-FRET, time resolved fluorescence energy transfer; TSA, Trichostatin A; UV detection, ultraviolet detection; ZMAL, Z-(Ac)Lys-AMC.

REFERENCES

1. Taunton, J.; Hassig, C. A.; Schreiber, S. L., A mammalian histone deacetylase related to the yeast transcriptional regulator Rpd3p. *Science* **1996**, 272 (5260), 408-11.
2. Kuo, M. H.; Allis, C. D., Roles of histone acetyltransferases and deacetylases in gene regulation. *Bioessays* **1998**, 20 (8), 615-26.
3. Leipe, D. D.; Landsman, D., Histone deacetylases, acetoin utilization proteins and acetylpolyamine amidohydrolases are members of an ancient protein superfamily. *Nucleic Acids Res* **1997**, 25 (18), 3693-7.
4. Yang, W. M.; Inouye, C.; Zeng, Y. Y.; Bearss, D.; Seto, E., Transcriptional repression by YY1 is mediated by interaction with a mammalian homolog of the yeast global regulator RPD3. *P Natl Acad Sci USA* **1996**, 93 (23), 12845-12850.
5. Luo, J.; Su, F.; Chen, D.; Shiloh, A.; Gu, W., Deacetylation of p53 modulates its effect on cell growth and apoptosis. *Nature* **2000**, 408 (6810), 377-81.
6. Hubbert, C.; Guardiola, A.; Shao, R.; Kawaguchi, Y.; Ito, A.; Nixon, A.; Yoshida, M.; Wang, X. F.; Yao, T. P., HDAC6 is a microtubule-associated deacetylase. *Nature* **2002**, 417 (6887), 455-8.
7. Chakrabarti, A.; Melesina, J.; Kolbinger, F. R.; Oehme, I.; Senger, J.; Witt, O.; Sippl, W.; Jung, M., Targeting histone deacetylase 8 as a therapeutic approach to cancer and neurodegenerative diseases. *Future Med Chem* **2016**, 8 (13), 1609-34.
8. Kovacs, J. J.; Murphy, P. J.; Gaillard, S.; Zhao, X.; Wu, J. T.; Nicchitta, C. V.; Yoshida, M.; Toft, D. O.; Pratt, W. B.; Yao, T. P., HDAC6 regulates Hsp90 acetylation and chaperone-dependent activation of glucocorticoid receptor. *Mol Cell* **2005**, 18 (5), 601-7.
9. Wilson, B. J.; Tremblay, A. M.; Deblois, G.; Sylvain-Drolet, G.; Giguere, V., An acetylation switch modulates the transcriptional activity of estrogen-related receptor alpha. *Mol Endocrinol* **2010**, 24 (7), 1349-58.
10. Gregoret, I. V.; Lee, Y. M.; Goodson, H. V., Molecular evolution of the histone deacetylase family: functional implications of phylogenetic analysis. *J Mol Biol* **2004**, 338 (1), 17-31.
11. Kutil, Z.; Novakova, Z.; Melesin, M.; Mikesova, J.; Schutkowski, M.; Barinka, C., Histone Deacetylase 11 Is a Fatty-Acid Deacylase. *ACS Chem Biol* **2018**, 13 (3), 685-693.
12. Moreno-Yruela, C.; Galleano, I.; Madsen, A. S.; Olsen, C. A., Histone Deacetylase 11 Is an epsilon-N-Myristoyllysine Hydrolase. *Cell Chem Biol* **2018**, 25 (7), 849-856 e8.
13. Hai, Y.; Shinsky, S. A.; Porter, N. J.; Christianson, D. W., Histone deacetylase 10 structure and molecular function as a polyamine deacetylase. *Nature Communications* **2017**, 8.
14. Mihaylova, M. M.; Vasquez, D. S.; Ravnskjaer, K.; Denechaud, P. D.; Yu, R. T.; Alvarez, J. G.; Downes, M.; Evans, R. M.; Montminy, M.; Shaw, R. J., Class IIa Histone Deacetylases Are Hormone-Activated Regulators of FOXO and Mammalian Glucose Homeostasis. *Cell* **2011**, 145 (4), 607-621.
15. Qian, H.; Chen, Y. Y.; Nian, Z. Q.; Su, L.; Yu, H. Y.; Chen, F. J.; Zhang, X. Q.; Xu, W. Y.; Zhou, L. K.; Liu, J. M.; Yu, J. H.; Yu, L. X.; Gao, Y.; Zhang, H. C.; Zhang, H. H.; Zhao, S. M.; Yu, L.; Xiao, R. P.; Bao, Y. Q.; Hou, S. C.; Li, P. P.; Li, J. D.; Deng, H. T.; Jia, W. P.; Li, P., HDAC6-mediated acetylation of lipid droplet-binding protein CIDEC regulates fat-induced lipid storage. *Journal of Clinical Investigation* **2017**, 127 (4), 1353-1369.

16. Song, S. Y.; Wen, Y. F.; Tong, H.; Loro, E.; Gong, Y. Y.; Liu, J. D.; Hong, S. G.; Li, L.; Khurana, T. S.; Chu, M. P.; Sun, Z., The HDAC3 enzymatic activity regulates skeletal muscle fuel metabolism. *J Mol Cell Biol* **2019**, *11* (2), 133-143.
17. Sen, P.; Shah, P. P.; Nativio, R.; Berger, S. L., Epigenetic Mechanisms of Longevity and Aging. *Cell* **2016**, *166* (4), 822-839.
18. Gallinari, P.; Di Marco, S.; Jones, P.; Pallaoro, M.; Steinkuhler, C., HDACs, histone deacetylation and gene transcription: from molecular biology to cancer therapeutics. *Cell Res* **2007**, *17* (3), 195-211.
19. Lai, I. L.; Lin, T. P.; Yao, Y. L.; Lin, C. Y.; Hsieh, M. J.; Yang, W. M., Histone deacetylase 10 relieves repression on the melanogenic program by maintaining the deacetylation status of repressors. *J Biol Chem* **2010**, *285* (10), 7187-96.
20. Wang, Z.; Zang, C.; Cui, K.; Schones, D. E.; Barski, A.; Peng, W.; Zhao, K., Genome-wide mapping of HATs and HDACs reveals distinct functions in active and inactive genes. *Cell* **2009**, *138* (5), 1019-31.
21. Kotian, S.; Liyanarachchi, S.; Zelent, A.; Parvin, J. D., Histone deacetylases 9 and 10 are required for homologous recombination. *J Biol Chem* **2011**, *286* (10), 7722-6.
22. Robert, T.; Vanoli, F.; Chiolo, I.; Shubassi, G.; Bernstein, K. A.; Rothstein, R.; Botrugno, O. A.; Parazzoli, D.; Oldani, A.; Minucci, S.; Foiani, M., HDACs link the DNA damage response, processing of double-strand breaks and autophagy. *Nature* **2011**, *471* (7336), 74-79.
23. Zhang, R. H.; Lu, J. Y.; Kong, X. Q.; Jin, L.; Luo, C., Targeting Epigenetics in Nervous System Disease. *Cns Neurol Disord-Dr* **2013**, *12* (1), 126-141.
24. Graff, J.; Rei, D.; Guan, J. S.; Wang, W. Y.; Seo, J.; Hennig, K. M.; Nieland, T. J. F.; Fass, D. M.; Kao, P. F.; Kahn, M.; Su, S. C.; Samiei, A.; Joseph, N.; Haggarty, S. J.; Delalle, I.; Tsai, L. H., An epigenetic blockade of cognitive functions in the neurodegenerating brain. *Nature* **2012**, *483* (7388), 222-U123.
25. Miao, F.; Gonzalo, I. G.; Lanting, L.; Natarajan, R., In vivo chromatin remodeling events leading to inflammatory gene transcription under diabetic conditions. *Journal of Biological Chemistry* **2004**, *279* (17), 18091-18097.
26. Sun, L.; de Evsikova, C. M.; Bian, K.; Achille, A.; Telles, E.; Pei, H. D.; Seto, E., Programming and Regulation of Metabolic Homeostasis by HDAC11. *Ebiomedicine* **2018**, *33*, 157-168.
27. Oehme, I.; Lodrini, M.; Brady, N. R.; Witt, O., Histone deacetylase 10-promoted autophagy as a druggable point of interference to improve the treatment response of advanced neuroblastomas. *Autophagy* **2013**, *9* (12), 2163-5.
28. Nakagawa, M.; Oda, Y.; Eguchi, T.; Aishima, S.; Yao, T.; Hosoi, F.; Basaki, Y.; Ono, M.; Kuwano, M.; Tanaka, M.; Tsuneyoshi, M., Expression profile of class I histone deacetylases in human cancer tissues. *Oncol Rep* **2007**, *18* (4), 769-74.
29. Wilson, A. J.; Byun, D. S.; Popova, N.; Murray, L. B.; L'Italien, K.; Sowa, Y.; Arango, D.; Velcich, A.; Augenlicht, L. H.; Mariadason, J. M., Histone deacetylase 3 (HDAC3) and other class I HDACs regulate colon cell maturation and p21 expression and are deregulated in human colon cancer. *J Biol Chem* **2006**, *281* (19), 13548-58.
30. Song, C. L.; Zhu, S. C.; Wu, C. Y.; Kang, J. H., Histone Deacetylase (HDAC) 10 Suppresses Cervical Cancer Metastasis through Inhibition of Matrix Metalloproteinase (MMP) 2 and 9 Expression. *Journal of Biological Chemistry* **2013**, *288* (39), 28021-28033.

31. Wu, J.; Du, C.; Lv, Z.; Ding, C.; Cheng, J.; Xie, H.; Zhou, L.; Zheng, S., The up-regulation of histone deacetylase 8 promotes proliferation and inhibits apoptosis in hepatocellular carcinoma. *Dig Dis Sci* **2013**, *58* (12), 3545-53.
32. Duan, B. Y.; Ye, D.; Zhu, S. C.; Jia, W. W.; Lu, C. Q.; Wang, G. Y.; Guo, X. D.; Yu, Y. Y.; Wu, C. Y.; Kang, J. H., HDAC10 promotes angiogenesis in endothelial cells through the PTPN22/ERK axis. *Oncotarget* **2017**, *8* (37), 61338-61349.
33. Oehme, I.; Linke, J. P.; Bock, B. C.; Milde, T.; Lodrini, M.; Hartenstein, B.; Wiegand, I.; Eckert, C.; Roth, W.; Kool, M.; Kaden, S.; Grone, H. J.; Schulte, J. H.; Lindner, S.; Hamacher-Brady, A.; Brady, N. R.; Deubzer, H. E.; Witt, O., Histone deacetylase 10 promotes autophagy-mediated cell survival. *Proc Natl Acad Sci U S A* **2013**, *110* (28), E2592-601.
34. Ridinger, J.; Koenke, E.; Kolbinger, F. R.; Koerholz, K.; Mahboobi, S.; Hellweg, L.; Gunkel, N.; Miller, A. K.; Peterziel, H.; Schmezer, P.; Hamacher-Brady, A.; Witt, O.; Oehme, I., Dual role of HDAC10 in lysosomal exocytosis and DNA repair promotes neuroblastoma chemoresistance. *Sci Rep* **2018**, *8* (1), 10039.
35. Yang, Y. W.; Huang, Y. T.; Wang, Z. T.; Wang, H. T.; Duan, B. Y.; Ye, D.; Wang, C. X.; Jing, R. Q.; Leng, Y.; Xi, J. J.; Chen, W.; Wang, G. Y.; Jia, W. W.; Zhu, S. C.; Kang, J. H., HDAC10 promotes lung cancer proliferation via AKT phosphorylation. *Oncotarget* **2016**, *7* (37), 59388-59401.
36. Shan, C. L.; Lu, Z. L.; Li, Z.; Sheng, H.; Fan, J.; Qi, Q.; Liu, S. P.; Zhang, S., 4-hydroxyphenylpyruvate dioxygenase promotes lung cancer growth via pentose phosphate pathway (PPP) flux mediated by LKB1-AMPK/HDAC10/G6PD axis. *Cell Death Dis* **2019**, *10*.
37. Islam, M. M.; Banerjee, T.; Packard, C. Z.; Kotian, S.; Selvendiran, K.; Cohn, D. E.; Parvin, J. D., HDAC10 as a potential therapeutic target in ovarian cancer. *Gynecol Oncol* **2017**, *144* (3), 613-620.
38. Yoshida, M.; Kijima, M.; Akita, M.; Beppu, T., Potent and specific inhibition of mammalian histone deacetylase both in vivo and in vitro by trichostatin A. *J Biol Chem* **1990**, *265* (28), 17174-9.
39. Kijima, M.; Yoshida, M.; Sugita, K.; Horinouchi, S.; Beppu, T., Trapoxin, an Antitumor Cyclic Tetrapeptide, Is an Irreversible Inhibitor of Mammalian Histone Deacetylase. *Journal of Biological Chemistry* **1993**, *268* (30), 22429-22435.
40. Duvic, M.; Vu, J., Vorinostat: a new oral histone deacetylase inhibitor approved for cutaneous T-cell lymphoma. *Expert Opin Investig Drugs* **2007**, *16* (7), 1111-20.
41. Furumai, R.; Matsuyama, A.; Kobashi, N.; Lee, K. H.; Nishiyama, N.; Nakajima, I.; Tanaka, A.; Komatsu, Y.; Nishino, N.; Yoshida, M.; Horinouchi, S., FK228 (depsipeptide) as a natural prodrug that inhibits class I histone deacetylases. *Cancer Research* **2002**, *62* (17), 4916-4921.
42. Lee, H. Z.; Kwitkowski, V. E.; Del Valle, P. L.; Ricci, M. S.; Saber, H.; Habtemariam, B. A.; Bullock, J.; Bloomquist, E.; Li Shen, Y.; Chen, X. H.; Brown, J.; Mehrotra, N.; Dorff, S.; Charlab, R.; Kane, R. C.; Kaminskis, E.; Justice, R.; Farrell, A. T.; Pazdur, R., FDA Approval: Belinostat for the Treatment of Patients with Relapsed or Refractory Peripheral T-cell Lymphoma. *Clin Cancer Res* **2015**, *21* (12), 2666-70.
43. Raedler, L. A., Farydak (Panobinostat): First HDAC Inhibitor Approved for Patients with Relapsed Multiple Myeloma. *Am Health Drug Benefits* **2016**, *9* (Spec Feature), 84-7.
44. Richon, V. M.; Emiliani, S.; Verdin, E.; Webb, Y.; Breslow, R.; Rifkind, R. A.; Marks, P. A., A class of hybrid polar inducers of transformed cell differentiation inhibits histone deacetylases. *P Natl Acad Sci USA* **1998**, *95* (6), 3003-3007.

45. Lu, X.; Ning, Z.; Li, Z.; Cao, H.; Wang, X., Development of chidamide for peripheral T-cell lymphoma, the first orphan drug approved in China. *Intractable Rare Dis Res* **2016**, *5* (3), 185-91.
46. Tjulandin, S.; Fedyanin, M.; Vladimirov, V. I.; Kostorov, V.; Lisyanskaya, A. S.; Krikunova, L.; Cakana, A.; Azarova, V.; Karavaeva, O.; Vostokova, N.; Baranovsky, S., A multicenter phase II study of the efficacy and safety of quisinostat (an HDAC inhibitor) in combination with paclitaxel and carboplatin chemotherapy (CT) in patients (pts) with recurrent platinum resistant high grade serous epithelial ovarian, primarily peritoneal or fallopian tube carcinoma cancer (OC). *J Clin Oncol* **2017**, *35*.
47. Aggarwal, R. R.; Thomas, S.; Hauke, R. J.; Nordquist, L. T.; Munster, P. N., RENAVIV: A randomized phase III, double-blind, placebo-controlled study of pazopanib with or without abexinostat in patients with locally advanced or metastatic renal cell carcinoma. *J Clin Oncol* **2019**, *37* (7).
48. Batlevi, C. L.; Crump, M.; Andreadis, C.; Rizzieri, D.; Assouline, S. E.; Fox, S.; van der Jagt, R. H. C.; Copeland, A.; Potvin, D.; Chao, R.; Younes, A., A phase 2 study of mocetinostat, a histone deacetylase inhibitor, in relapsed or refractory lymphoma. *Brit J Haematol* **2017**, *178* (3), 434-441.
49. Balasubramanian, S.; Verner, E.; Buggy, J. J., Isoform-specific histone deacetylase inhibitors: the next step? *Cancer Lett* **2009**, *280* (2), 211-21.
50. Marek, L.; Hamacher, A.; Hansen, F. K.; Kuna, K.; Gohlke, H.; Kassack, M. U.; Kurz, T., Histone Deacetylase (HDAC) Inhibitors with a Novel Connecting Unit Linker Region Reveal a Selectivity Profile for HDAC4 and HDAC5 with Improved Activity against Chemoresistant Cancer Cells. *Journal of Medicinal Chemistry* **2013**, *56* (2), 427-436.
51. Martin, M. W.; Lee, J. Y.; Lancia, D. R.; Ng, P. Y.; Han, B. S.; Thomason, J. R.; Lynes, M. S.; Marshall, C. G.; Conti, C.; Collis, A.; Morales, M. A.; Doshi, K.; Rudnitskaya, A.; Yao, L. L.; Zheng, X. Z., Discovery of novel N-hydroxy-2-arylisoindoline-4-carboxamides as potent and selective inhibitors of HDAC11. *Bioorganic & Medicinal Chemistry Letters* **2018**, *28* (12), 2143-2147.
52. Zhang, Y.; Yan, J.; Yao, T. P., Discovery of a fluorescent probe with HDAC6 selective inhibition. *Eur J Med Chem* **2017**, *141*, 596-602.
53. Roche, J.; Bertrand, P., Inside HDACs with more selective HDAC inhibitors. *Eur J Med Chem* **2016**, *121*, 451-483.
54. Hai, Y.; Christianson, D. W., Histone deacetylase 6 structure and molecular basis of catalysis and inhibition. *Nat Chem Biol* **2016**, *12* (9), 741-7.
55. Li, J.; Staver, M. J.; Curtin, M. L.; Holms, J. H.; Frey, R. R.; Edalji, R.; Smith, R.; Michaelides, M. R.; Davidsen, S. K.; Glaser, K. B., Expression and functional characterization of recombinant human HDAC1 and HDAC3. *Life Sci* **2004**, *74* (22), 2693-705.
56. Jones, P.; Altamura, S.; De Francesco, R.; Gallinari, P.; Lahm, A.; Neddermann, P.; Rowley, M.; Serafini, S.; Steinkuhler, C., Probing the elusive catalytic activity of vertebrate class IIa histone deacetylases. *Bioorg Med Chem Lett* **2008**, *18* (6), 1814-9.
57. Marks, B. D.; Fakhoury, S. A.; Frazee, W. J.; Eliason, H. C.; Riddle, S. M., A Substrate-Independent TR-FRET Histone Deacetylase Inhibitor Assay. *J Biomol Screen* **2011**, *16* (10), 1247-1253.
58. Robers, M. B.; Dart, M. L.; Woodroffe, C. C.; Zimprich, C. A.; Kirkland, T. A.; Machleidt, T.; Kupcho, K. R.; Levin, S.; Hartnett, J. R.; Zimmerman, K.; Niles, A. L.; Ohana, R. F.; Daniels, D. L.; Slater, M.; Wood, M. G.; Cong, M.; Cheng, Y. Q.; Wood, K. V., Target

engagement and drug residence time can be observed in living cells with BRET. *Nature Communications* **2015**, *6*.

59. De Vreese, R.; D'Hooghe, M., Synthesis and applications of benzohydroxamic acid-based histone deacetylase inhibitors. *Eur J Med Chem* **2017**, *135*, 174-195.
60. Gerald, M.; Morgen, M.; Sehr, P.; Steimbach, R. R.; Moi, D.; Ridinger, J.; Oehme, I.; Witt, O.; Malz, M.; Nogueira, M. S.; Koch, O.; Gunkel, N.; Miller, A. K., Selective Inhibition of Histone Deacetylase 10: Hydrogen Bonding to the Gatekeeper Residue is Implicated. *J Med Chem* **2019**, *62* (9), 4426-4443.
61. Uba, A. I.; Yelekci, K., Crystallographic structure versus homology model: a case study of molecular dynamics simulation of human and zebrafish histone deacetylase 10. *J Biomol Struct Dyn* **2019**, 1-12.
62. Ibrahim Uba, A.; Yelekci, K., Homology modeling of human histone deacetylase 10 and design of potential selective inhibitors. *J Biomol Struct Dyn* **2019**, *37* (14), 3627-3636.
63. Herbst-Gervasoni, C. J.; Christianson, D. W., Binding of N8-Acetylspermidine Analogues to Histone Deacetylase 10 Reveals Molecular Strategies for Blocking Polyamine Deacetylation. *Biochemistry-Us* **2019**.
64. Heltweg, B.; Jung, M., A homogeneous nonisotopic histone deacetylase activity assay. *J Biomol Screen* **2003**, *8* (1), 89-95.
65. Demontigny, P.; Stobaugh, J. F.; Givens, R. S.; Carlson, R. G.; Srinivasachar, K.; Sternson, L. A.; Higuchi, T., Naphthalene-2,3-Dicarboxaldehyde Cyanide Ion - a Rationally Designed Fluorogenic Reagent for Primary Amines. *Analytical Chemistry* **1987**, *59* (8), 1096-1101.
66. Zhang, J. H.; Chung, T. D. Y.; Oldenburg, K. R., A simple statistical parameter for use in evaluation and validation of high throughput screening assays. *J Biomol Screen* **1999**, *4* (2), 67-73.
67. Bantscheff, M.; Hopf, C.; Savitski, M. M.; Dittmann, A.; Grandi, P.; Michon, A. M.; Schlegl, J.; Abraham, Y.; Becher, I.; Bergamini, G.; Boesche, M.; Delling, M.; Dumpelfeld, B.; Eberhard, D.; Huthmacher, C.; Mathieson, T.; PoECKel, D.; Reader, V.; Strunk, K.; Sweetman, G.; Kruse, U.; Neubauer, G.; Ramsden, N. G.; Drewes, G., Chemoproteomics profiling of HDAC inhibitors reveals selective targeting of HDAC complexes. *Nat Biotechnol* **2011**, *29* (3), 255-U124.
68. Wagner, F. F.; Olson, D. E.; Gale, J. P.; Kaya, T.; Weiwer, M.; Aidoud, N.; Thomas, M.; Davoine, E. L.; Lemercier, B. C.; Zhang, Y. L.; Holson, E. B., Potent and selective inhibition of histone deacetylase 6 (HDAC6) does not require a surface-binding motif. *J Med Chem* **2013**, *56* (4), 1772-6.
69. Balasubramanian, S.; Ramos, J.; Luo, W.; Sirisawad, M.; Verner, E.; Buggy, J. J., A novel histone deacetylase 8 (HDAC8)-specific inhibitor PCI-34051 induces apoptosis in T-cell lymphomas. *Leukemia* **2008**, *22* (5), 1026-1034.
70. Fournel, M.; Bonfils, C.; Hou, Y.; Yan, P. T.; Trachy-Bourget, M. C.; Kalita, A.; Liu, J.; Lu, A. H.; Zhou, N. Z.; Robert, M. F.; Gillespie, J.; Wang, J. J.; Ste-Croix, H.; Rahil, J.; Lefebvre, S.; Moradei, O.; Delorme, D.; MacLeod, A. R.; Besterman, J. M.; Li, Z. M., MGCD0103, a novel isotype-selective histone deacetylase inhibitor, has broad spectrum antitumor activity in vitro and in vivo. *Mol Cancer Ther* **2008**, *7* (4), 759-768.
71. Bayer, T.; Chakrabarti, A.; Lancelot, J.; Shaik, T. B.; Hausmann, K.; Melesina, J.; Schmidtkunz, K.; Marek, M.; Erdmann, F.; Schmidt, M.; Robaa, D.; Romier, C.; Pierce, R. J.; Jung, M.; Sippl, W., Synthesis, Crystallization Studies, and in vitro Characterization of Cinnamic

Acid Derivatives as SmHDAC8 Inhibitors for the Treatment of Schistosomiasis. *ChemMedChem* **2018**, *13* (15), 1517-1529.

72. Heimburg, T.; Kolbinger, F. R.; Zeyen, P.; Ghazy, E.; Herp, D.; Schmidtkunz, K.; Melesina, J.; Shaik, T. B.; Erdmann, F.; Schmidt, M.; Romier, C.; Robaa, D.; Witt, O.; Oehme, I.; Jung, M.; Sippl, W., Structure-Based Design and Biological Characterization of Selective Histone Deacetylase 8 (HDAC8) Inhibitors with Anti-Neuroblastoma Activity. *J Med Chem* **2017**, *60* (24), 10188-10204.
73. Senger, J.; Melesina, J.; Marek, M.; Romier, C.; Oehme, I.; Witt, O.; Sippl, W.; Jung, M., Synthesis and Biological Investigation of Oxazole Hydroxamates as Highly Selective Histone Deacetylase 6 (HDAC6) Inhibitors. *J Med Chem* **2016**, *59* (4), 1545-55.
74. Schaefer, S.; Saunders, L.; Schlimme, S.; Valkov, V.; Wagner, J. M.; Kratz, F.; Sippl, W.; Verdin, E.; Jung, M., Pyridylalanine-Containing Hydroxamic Acids as Selective HDAC6 Inhibitors. *Chemmedchem* **2009**, *4* (2), 283-290.
75. Jung, M.; Brosch, G.; Kolle, D.; Scherf, H.; Gerhauser, C.; Loidl, P., Amide analogues of trichostatin A as inhibitors of histone deacetylase and inducers of terminal cell differentiation. *Journal of Medicinal Chemistry* **1999**, *42* (22), 4669-4679.
76. Uesato, S.; Kitagawa, M.; Nagaoka, Y.; Maeda, T.; Kuwajima, H.; Yamori, T., Novel histone deacetylase inhibitors: N-hydroxycarboxamides possessing a terminal bicyclic aryl group. *Bioorg Med Chem Lett* **2002**, *12* (10), 1347-9.
77. Herbst-Gervasoni, C. J.; Christianson, D. W., Binding of N(8)-Acetylspermidine Analogues to Histone Deacetylase 10 Reveals Molecular Strategies for Blocking Polyamine Deacetylation. *Biochemistry-Us* **2019**, *58* (49), 4957-4969.
78. Watson, P. J.; Millard, C. J.; Riley, A. M.; Robertson, N. S.; Wright, L. C.; Godage, H. Y.; Cowley, S. M.; Jamieson, A. G.; Potter, B. V.; Schwabe, J. W., Insights into the activation mechanism of class I HDAC complexes by inositol phosphates. *Nat Commun* **2016**, *7*, 11262.
79. Vannini, A.; Volpari, C.; Gallinari, P.; Jones, P.; Mattu, M.; Carfi, A.; De Francesco, R.; Steinkuhler, C.; Di Marco, S., Substrate binding to histone deacetylases as shown by the crystal structure of the HDAC8-substrate complex. *EMBO Rep* **2007**, *8* (9), 879-84.
80. Miyake, Y.; Keusch, J. J.; Wang, L.; Saito, M.; Hess, D.; Wang, X.; Melancon, B. J.; Helquist, P.; Gut, H.; Matthias, P., Structural insights into HDAC6 tubulin deacetylation and its selective inhibition. *Nat Chem Biol* **2016**, *12* (9), 748-54.
81. Porter, N. J.; Osko, J. D.; Diedrich, D.; Kurz, T.; Hooker, J. M.; Hansen, F. K.; Christianson, D. W., Histone Deacetylase 6-Selective Inhibitors and the Influence of Capping Groups on Hydroxamate-Zinc Denticity. *J Med Chem* **2018**, *61* (17), 8054-8060.
82. Osko, J. D.; Porter, N. J.; Narayana Reddy, P. A.; Xiao, Y. C.; Rokka, J.; Jung, M.; Hooker, J. M.; Salvino, J. M.; Christianson, D. W., Exploring Structural Determinants of Inhibitor Affinity and Selectivity in Complexes with Histone Deacetylase 6. *J Med Chem* **2020**, *63* (1), 295-308.
83. Porter, N. J.; Mahendran, A.; Breslow, R.; Christianson, D. W., Unusual zinc-binding mode of HDAC6-selective hydroxamate inhibitors. *Proc Natl Acad Sci U S A* **2017**, *114* (51), 13459-13464.
84. Shen, S.; Svoboda, M.; Zhang, G.; Cavasin, M. A.; Motlova, L.; McKinsey, T. A.; Eubanks, J. H.; Bařinka, C.; Kozikowski, A. P., Structural and in Vivo Characterization of Tubastatin A, a Widely Used Histone Deacetylase 6 Inhibitor. *ACS Medicinal Chemistry Letters* **2020**.

85. Porter, N. J.; Wagner, F. F.; Christianson, D. W., Entropy as a Driver of Selectivity for Inhibitor Binding to Histone Deacetylase 6. *Biochemistry* **2018**, *57* (26), 3916-3924.
86. Osko, J. D.; Christianson, D. W., Structural determinants of affinity and selectivity in the binding of inhibitors to histone deacetylase 6. *Bioorg Med Chem Lett* **2020**, *30* (8), 127023.
87. Heimbürg, T.; Chakrabarti, A.; Lancelot, J.; Marek, M.; Melesina, J.; Hauser, A. T.; Shaik, T. B.; Duclaud, S.; Robaa, D.; Erdmann, F.; Schmidt, M.; Romier, C.; Pierce, R. J.; Jung, M.; Sippl, W., Structure-Based Design and Synthesis of Novel Inhibitors Targeting HDAC8 from *Schistosoma mansoni* for the Treatment of Schistosomiasis. *J Med Chem* **2016**, *59* (6), 2423-35.
88. Marek, M.; Shaik, T. B.; Heimbürg, T.; Chakrabarti, A.; Lancelot, J.; Ramos-Morales, E.; Da Veiga, C.; Kalinin, D.; Melesina, J.; Robaa, D.; Schmidtkunz, K.; Suzuki, T.; Holl, R.; Ennifar, E.; Pierce, R. J.; Jung, M.; Sippl, W.; Romier, C., Characterization of Histone Deacetylase 8 (HDAC8) Selective Inhibition Reveals Specific Active Site Structural and Functional Determinants. *Journal of medicinal chemistry* **2018**, *61* (22), 10000-10016.
89. Butler, K. V.; Kalin, J.; Brochier, C.; Vistoli, G.; Langley, B.; Kozikowski, A. P., Rational design and simple chemistry yield a superior, neuroprotective HDAC6 inhibitor, tubastatin A. *J Am Chem Soc* **2010**, *132* (31), 10842-6.
90. Heltweg, B.; Trapp, J.; Jung, M., In vitro assays for the determination of histone deacetylase activity. *Methods* **2005**, *36* (4), 332-337.
91. Marek, M.; Kannan, S.; Hauser, A. T.; Moraes Mourao, M.; Caby, S.; Cura, V.; Stolfa, D. A.; Schmidtkunz, K.; Lancelot, J.; Andrade, L.; Renaud, J. P.; Oliveira, G.; Sippl, W.; Jung, M.; Cavarelli, J.; Pierce, R. J.; Romier, C., Structural basis for the inhibition of histone deacetylase 8 (HDAC8), a key epigenetic player in the blood fluke *Schistosoma mansoni*. *PLoS Pathog* **2013**, *9* (9), e1003645.
92. Hai, Y.; Shinsky, S. A.; Porter, N. J.; Christianson, D. W., Histone deacetylase 10 structure and molecular function as a polyamine deacetylase. *Nat Commun* **2017**, *8*, 15368.
93. Banks, J. L.; Beard, H. S.; Cao, Y.; Cho, A. E.; Damm, W.; Farid, R.; Felts, A. K.; Halgren, T. A.; Mainz, D. T.; Maple, J. R.; Murphy, R.; Philipp, D. M.; Repasky, M. P.; Zhang, L. Y.; Berne, B. J.; Friesner, R. A.; Gallicchio, E.; Levy, R. M., Integrated Modeling Program, Applied Chemical Theory (IMPACT). *J Comput Chem* **2005**, *26* (16), 1752-80.
94. Watts, K. S.; Dalal, P.; Murphy, R. B.; Sherman, W.; Friesner, R. A.; Shelley, J. C., ConfGen: a conformational search method for efficient generation of bioactive conformers. *J Chem Inf Model* **2010**, *50* (4), 534-46.
95. Burley, S. K.; Berman, H. M.; Christie, C.; Duarte, J. M.; Feng, Z.; Westbrook, J.; Young, J.; Zardecki, C., RCSB Protein Data Bank: Sustaining a living digital data resource that enables breakthroughs in scientific research and biomedical education. *Protein Sci* **2018**, *27* (1), 316-330.
96. Sastry, G. M.; Adzhigirey, M.; Day, T.; Annabhimoju, R.; Sherman, W., Protein and ligand preparation: parameters, protocols, and influence on virtual screening enrichments. *J Comput Aided Mol Des* **2013**, *27* (3), 221-34.
97. Shelley, J. C.; Cholleti, A.; Frye, L. L.; Greenwood, J. R.; Timlin, M. R.; Uchimaya, M., Epik: a software program for pK(a) prediction and protonation state generation for drug-like molecules. *J Comput Aided Mol Des* **2007**, *21* (12), 681-91.
98. Halgren, T. A.; Murphy, R. B.; Friesner, R. A.; Beard, H. S.; Frye, L. L.; Pollard, W. T.; Banks, J. L., Glide: a new approach for rapid, accurate docking and scoring. 2. Enrichment factors in database screening. *J Med Chem* **2004**, *47* (7), 1750-9.

99. Friesner, R. A.; Banks, J. L.; Murphy, R. B.; Halgren, T. A.; Klicic, J. J.; Mainz, D. T.; Repasky, M. P.; Knoll, E. H.; Shelley, M.; Perry, J. K.; Shaw, D. E.; Francis, P.; Shenkin, P. S., Glide: a new approach for rapid, accurate docking and scoring. 1. Method and assessment of docking accuracy. *J Med Chem* **2004**, *47* (7), 1739-49.
100. Baell, J. B.; Holloway, G. A., New Substructure Filters for Removal of Pan Assay Interference Compounds (PAINS) from Screening Libraries and for Their Exclusion in Bioassays. *Journal of Medicinal Chemistry* **2010**, *53* (7), 2719-2740.

For Table of Contents Only

